

The Search for Failed Supernovae with The Large Binocular Telescope: First Candidates

J. R. Gerke¹, C. S. Kochanek^{1,2}, K. Z. Stanek^{1,2}

¹*Department of Astronomy, The Ohio State University, 140 West 18th Avenue, Columbus OH 43210*

²*Center for Cosmology and AstroParticle Physics, The Ohio State University, 191 W. Woodruff Avenue, Columbus OH 43210*

10 April 2015

ABSTRACT

We are monitoring 27 galaxies within 10 Mpc using the Large Binocular Telescope to search for failed supernovae (SNe), massive stars that collapse to form a black hole without a SN explosion. We present the results from the first 4 years of survey data, during which these galaxies were observed to produce 3 successful core-collapse SNe. We search for stars that have “vanished” over the course of our survey, by examining all stars showing a decrease in luminosity of $\Delta\nu L_\nu \geq 10^4 L_\odot$ from the first to the last observation. We also search for the low luminosity, long duration transients predicted by Lovegrove & Woosley (2013) for failed explosions of red supergiants. After analyzing the first 4 years of data in this first direct search for failed SNe, we are left with one candidate requiring further study. This candidate has an estimated mass of $18\text{--}25 M_\odot$, a mass range likely associated with failed SNe and, if real, implies that failed SN represent a median fraction of $f \simeq 0.30$ of core-collapses, with symmetric 90% confidence limits of $0.07 \leq f \leq 0.62$. If follow up data eliminate this candidate, we find an upper limit on the fraction of core collapses leading to a failed SN of $f < 0.40$ at 90% confidence. As the duration of the survey continues to increase, it will begin to constrain the $f \simeq 10\text{--}30\%$ failure rates needed to explain the deficit of massive SN progenitors and the observed black hole mass function.

Key words: stars:massive, supernovae:general, surveys:stars, black hole physics

1 INTRODUCTION

Massive stars have a tremendous impact on the evolution of galaxies and stellar populations through both energy injection and chemical enrichment. To understand how massive stars affect their environments, we must understand their deaths, particularly the balance between successful supernovae (SNe), which eject most of their mass, including significant amounts of nuclear processed material to be recycled into a new generation of stars, and failed SNe, which form a black hole while ejecting little or no energy or enriched material (see Smartt 2009 for a review of SN progenitors). Understanding this balance is also crucial to understanding the SN mechanism, a long standing problem in astronomy (see Pejcha & Thompson 2014).

It has long been believed that some fraction of massive stars experience a failed SN. The focus has usually been on high mass stars at lower metallicity where mass loss may be smaller (Heger et al. 2003). However, there are also arguments about whether elemental abundances require a significant fraction of failed SNe for $M \gtrsim 25 M_\odot$ to avoid the overproduction of heavy elements (e.g. Maeder 1992 for

and Prantzos 1994 against). Brown & Woosley (2013) find abundances are fit well with both no failed SNe and having all stars above $25 M_\odot$ experience a failed SN. Pushing the failed SN limit down to $18 M_\odot$ requires a star formation rate 3 times the fiducial value. However, they do not explore the consequences of failed SNe from a more complex range of masses other than a simple mass limit. Clausen et al. (2014) used a more physical model for the mass distribution of failed SNe and found only weak constraints on any mass range associated with failed SNe from abundance measurements.

The question of failed SNe has become more pressing because there appears to be a dearth of high mass SN progenitors (Kochanek et al. 2008). In particular, Smartt et al. (2009) find no Type IIP progenitors more massive than those corresponding to initial masses of $\simeq 18 M_\odot$, even though stars with initial masses up to $25\text{--}30 M_\odot$ are thought to explode as red supergiants (RSG). It is possible that this RSG problem has a solution other than failed SNe, such as different physical treatments in the stellar evolution models, as discussed by Smartt et al. (2009). For example, the rotating models of Groh et al. (2013) can move the upper mass limit

to explode as a red supergiant to as low as $17 M_{\odot}$, although these models may be in conflict with recent astroseismic results (Ceillier et al. 2012). Another option is to make these stars very dusty (Walmswell & Eldridge 2012), so that they would be fainter and thus have underestimated masses if the extinction is not well understood, although, these particular models overestimate the net effect (see Kochanek et al. 2012b). While the progenitor masses depend somewhat on the analysis (e.g., Maund et al. 2014), the basic conclusion of Kochanek et al. (2008) and Smartt et al. (2009) appears to be robust. Moreover, studies using local stellar populations to estimate progenitor masses of historical SNe have found similar results (Jennings et al. 2012; Williams et al. 2014; Jennings et al. 2014). Failed SNe in this mass range can also explain the black hole mass function (Kochanek 2014a,b) and the mismatch between star formation and SN rate estimates (Horiuchi et al. 2011, 2014).

We estimate that the failed ccSNe fraction f associated with the red supergiant problem is $f = 0.20$ with a crude 90% confidence range of $0.11 < f < 0.33$. We made this estimate by modeling the upper and lower mass limits for RSG core collapses using a Gaussian model for the Smartt et al. (2009) results, a uniform distribution from 25 to $30M_{\odot}$ for the upper mass limit of stars that are RSGs at death, and a uniform distribution from 100 to $200M_{\odot}$ for the upper mass limit of the IMF. If we disallow core collapse below $8-9M_{\odot}$, the lower limit rises to $f \simeq 0.15$. This range is very similar to the estimates of $f = 0.18$ ($0.09 < f < 0.39$) associated with explaining the black hole mass function using failed ccSNe (Kochanek 2015), although these limits fixed the minimum mass for core collapse to $9M_{\odot}$ and allow failed ccSNe of stripped stars as well as RSGs.

While simulations of SNe cannot at present predict which SN will succeed, they can explore which stars are more difficult to explode given their mass and internal structure. O’Connor & Ott (2011) used the compactness of the core at bounce to estimate whether a SN is likely to be successful. They find that progenitors in the mass range associated with the RSG problem also have structures that make them more difficult to explode. Ugliano et al. (2012) also found that this progenitor mass range is more likely to result in a failed SN. In their study of the neutrino mechanism for SNe, Pejcha & Thompson (2014) show that a number of mass ranges probably lead to failed SNe, again including the mass range associated with the RSG problem, and that a failure rate $f \simeq 20 - 30\%$ is quite probable. This is also supported by the black hole mass function (Kochanek 2014a,b).

Despite the expectation that some massive stars end their lives in a failed SN, there are surprisingly few studies of the external appearance of such events. Woosley & Heger (2012) found that some stars can collapse without fallback, probably forming a black hole without a significant transient. Failed SNe of RSGs probably produce a low luminosity optical transient. Lovegrove & Woosley (2013), motivated by Nadezhin (1980), simulated failed SNe of 15 and $25M_{\odot}$ RSGs, finding that the mass energy lost in neutrinos leads to a weak shock that unbinds the stellar envelope. The resulting black hole has the mass of the helium core, and this would naturally explain the compact remnant mass function (Kochanek 2014a,b; Clausen et al. 2014). The optical signature of such failed SNe is a shock breakout followed by a longer term transient. The shock breakout produces a

brighter (few $10^7 L_{\odot}$) optical transient, but it only lasts for 3-10 days (Piro 2013). The longer term transient is driven by the recombination of the unbound envelope of the star, leading to a transient that lasts about ~ 1 year with a luminosity of order $L_{bol} \sim 10^6 L_{\odot}$ and a temperature of ~ 4000 K at peak (Lovegrove & Woosley 2013). While conditions are ideal for dust formation, dust formation only occurs as the transient begins to fade and so affects the optical signature little (Kochanek 2014c). No matter what the intervening physics, the star must ultimately “vanish” in the optical (see Kochanek et al. 2008).

Traditionally, the search for failed SNe has focused on neutrinos (e.g., Lien et al. 2010; Mhlbeier et al. 2013) or gravitational waves (e.g., Ott 2009; Kotake 2011) with the difficulty that they could only be detected in the Milky Way with event timescales of centuries for a Galactic SN rate of 1 per 50 to 100 years (see Adams et al. 2013). However, in Kochanek et al. (2008) we pointed out that an optical survey for failed SNe was possible and could explore many more galaxies than simply the Milky Way. With an observed SN rate in the sample of ~ 1 per year, the time scales to detect a failed SN become much more practical. In essence, we are monitoring the health of $\sim 10^6$ RSGs in 27 galaxies within 10 Mpc using the Large Binocular Telescope (LBT) to see if any die, independent of the external symptoms beyond ultimately vanishing. With such a large sample of massive stars, we are able to probe the expected rates of this rare, difficult to observe phenomenon much more rapidly than if examining only our Galaxy.

In this work we report on the first such observational search for failed SNe. In §2 we discuss the galaxy sample and survey observations while §3 explains our image subtraction and calibration methods. In §4 we outline the candidate selection process and in §5 discuss the successful SNe in our sample. We discuss the last three rejected candidates in §6. In §7 we detail our remaining candidate and in §8 we place limits on the failed SN rate. We discuss future directions in §9 and summarize our results in §10.

2 GALAXY SAMPLE AND OBSERVATIONS

Our galaxy sample consists of 27 galaxies within 10 Mpc, essentially those selected in Kochanek et al. (2008) that are visible from the LBT (Hill et al. 2006) and their nearby companions. We do not include M31 and M33 because their sizes are poorly matched to our instrument. The galaxies and several of their properties are given in Table 1. The observing strategy made use of the LBT’s unique binocular feature, observing in the R Bessel filter with the red-optimized LBC-Red camera while simultaneously cycling through observations in the U_{spec} interference filter and the B and V Bessel filters with the blue optimized LBC-Blue camera (Giallongo et al. 2008). We calibrate our photometry to the Johnson-Cousins system, therefore we will refer to our calibrated R band magnitudes as R_c to differentiate from the filter. Additionally, the U_{spec} interference filter is very similar to the Bessel filter and we will refer to the calibrated magnitudes as U band. Each LBC camera consists of four 4096×2048 CCDs, each of which covers 17.3×7.7 arcmin² with a plate scale of $0''.225$ per pixel. Chips 1, 2 and 3 are adjacent to each other along the long sides of the

chips, while Chip 4 is above them and rotated by 90° (see Figure 4 in Giallongo et al. 2008), to provide a total area of roughly $23' \times 23'$. The majority of the target galaxies fit on the central chip, Chip 2. The larger galaxies required multiple chips: M81 (all chips), M101 (all chips), NGC 2403 (all chips), NGC 6946 (3 chips), NGC 628 (3 chips), NGC 4258 (2 chips) and NGC 672 (2 chips). A single pointing included NGC 3627 on Chip 3 and NGC 3628 on Chip 1. Another single pointing included NGC 4258 on Chip 2 and NGC 4248 on Chip 4.

Exposure times were chosen to try to reach a fixed point source luminosity limit for each galaxy, although in practice, we could not perfectly scale exposure times as the squared distance to the galaxies. Table 1 gives the theoretical depths from the LBC exposure time calculator for a signal-to-noise ratio (SNR) of $SNR = 5$ for the R band images and $1''$ seeing. These estimates agree well with individual observations (~ 0.1 mag). More importantly, we get an average of ~ 1 count per L_\odot (νL_ν in a band), so the massive stars we are interested in should be detectable with enough counts to monitor their variability. Figure 1 shows the expected R_c and U band luminosities of stars at the end of their lives based on Marigo et al. (2008) and Groh et al. (2013). The primary differences are due to the effects of mass loss on the effective temperatures. Most of the mass range of interest can be covered by a search for stars which change in luminosity by $\Delta \nu L_\nu > 10^4 L_\odot$. This will exclude the lowest mass progenitors, $\sim 10 M_\odot$, and higher mass progenitors that have been stripped to become Wolf-Rayet (WR). In all these models, however, stars in the $15\text{-}25 M_\odot$ range tend to have luminosities approaching $\nu L_\nu \sim 10^5 L_\odot$ in at least one of our survey bands. Hence we set the sensitivity goal for our survey to reach at least $\nu L_\nu > 10^4 L_\odot$ to include all the evolved stars expected to experience a SN that do not experience a high level of mass loss and become the stripped WR stars responsible for Type Ib and Ic SNe.

3 IMAGE SUBTRACTION AND CALIBRATION

The basic data reduction steps of overscan correction, bias subtraction, and flat fielding are preformed using the IRAF MSCRED package. While we collect data even in poor conditions on the grounds that an epoch in poor conditions is better than no epoch at all, here we only analyze images with $FWHM < 2''$. The median image quality is $1''.3$. Our search for stars in crowded fields showing large changes in luminosity is best accomplished by employing image subtraction. We use the ISIS image subtraction package (Alard & Lupton 1998; Alard 2000) to process our survey data.

We median combined a minimum of 3 of the best quality images (e.g. best FWHM, no cirrus, no moon) and on average used about 20% of the available images in the reference image. It is important to use many images to construct the reference image to minimize the noise it contributes to the subtracted images. The image subtraction is preformed by convolving the reference image with a kernel so that the psf structures of the observation and the reference image are matched. Because the reference image combines the best images, the noise and image quality of the subtracted image are dominated by the properties of the image being ana-

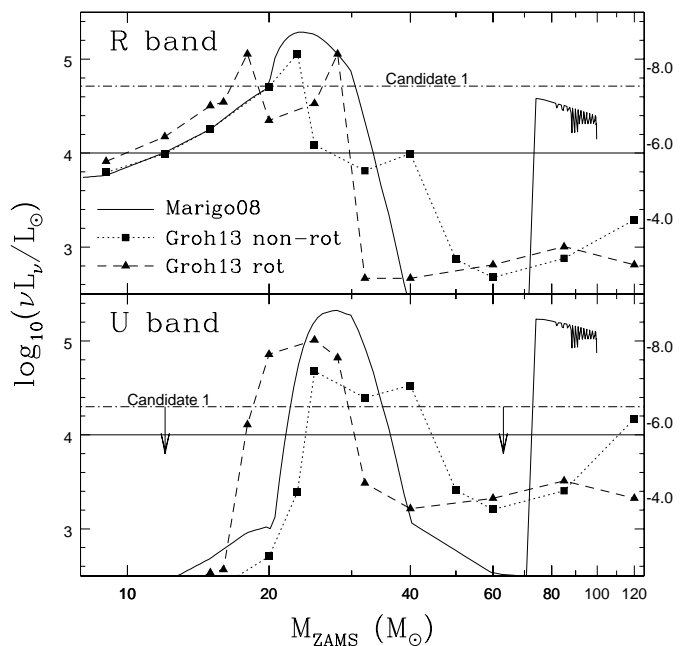


Figure 1. The expected R_c (top) and U (bottom) band luminosities of stars at the end of their lives based on Marigo et al. (2008) and Groh et al. (2013). The solid curves are for Marigo et al. (2008) and the dotted (dashed) lines are for the non-rotating (rotating) Groh et al. (2013) models. The vertical axis is in units of $\log(\nu L_\nu / L_\odot)$ on the left and absolute magnitude on the right. The horizontal axis is the zero-age main sequence (ZAMS) mass of a star. A horizontal line marks $\nu L_\nu \simeq 10^4 L_\odot$, our limit for identifying candidates. The luminosities of our remaining candidate, Candidate 1, are indicated by the horizontal dot-dashed lines.

lyzed rather than the reference image. Unfortunately the best seeing conditions were rare enough that we cannot, at this point, restrict the images used to construct the reference image to the second half of the survey, for example, and maintain the necessary quality of the reference image.

The R band reference image was used as the astrometric reference image for all four bands. By doing this, the UBV and R band images all have the same astrometric solution, and it becomes trivial to cross-match sources between bands. An astrometric solution was found for the majority of the galaxies using the IRAF package MSCCTPEAK and SDSS stars (Ivezić et al. 2007). There were 4 galaxies (NGC 6946, NGC 6503, NGC 925 and IC 2574) where we could not use SDSS to calibrate the reference images. Astrometric solutions for NGC 6946, NGC 925 and IC 2574 were found using the USNO-A2.0 catalog (Monet et al. 1998). The astrometric solution for NGC 6503 was found using the HST Guide Star Catalog 2.3 (Lasker et al. 2008). The typical residuals for the astrometric solutions are $\sim 0''.2$.

Most photometric calibrations were also based on SDSS. The SDSS photometry was transformed from the SDSS $ugriz$ filter system to the $UBVR_c$ system using the prescription described by Jordi et al. (2006). Thus, the final photometry consists of Vega magnitudes with the zeropoints as reported by Blanton & Roweis (2007). Again, there were 4 galaxies (NGC 6946, NGC 6503, NGC 925 and IC 2574) where we could not use SDSS to photometrically calibrate

Table 1. Galaxy Sample

Galaxy	Distance (Mpc)	Number of Epochs	Observation		Baseline (years)	$\nu L_\nu/L_\odot$ per Count	Depth R_c mag	Distance Reference
			First	Last				
M81	3.65	24	2008-03-08	2013-01-09	4.8	0.50	25.48	1
M82	3.52	16	2008-03-08	2013-01-10	4.8	1.11	25.43	2
M101	6.43	13	2008-03-08	2013-01-10	4.8	0.49	25.58	3
NGC 628	8.59	11	2009-01-31	2013-01-09	3.9	1.36	25.70	4
NGC 672	7.20	12	2008-07-05	2013-01-09	3.2	0.87	26.16	5
NGC 925	9.16	12	2008-07-06	2013-01-09	3.2	1.44	26.16	6
NGC 2403	3.56	23	2008-05-05	2013-01-10	3.9	0.48	26.24	7
NGC 2903	8.90	9	2008-03-08	2013-01-09	4.7	1.04	25.49	8
NGC 3077	3.82	10	2008-05-04	2013-01-10	3.9	0.48	26.10	5
NGC 3344	6.90	7	2008-05-04	2012-03-23	3.9	0.84	26.23	9
NGC 3489	7.18	6	2008-03-12	2012-03-23	4.0	1.14	26.28	10
NGC 3627	10.62	7	2008-05-04	2012-04-28	3.2	3.32	25.43	11
NGC 3628	10.62	7	2008-05-04	2012-04-28	3.2	3.48	25.43	11
NGC 4214	2.98	5	2008-03-13	2013-01-10	3.8	0.29	25.60	12
NGC 4236	3.65	7	2008-03-09	2013-01-10	3.9	0.34	26.10	1
NGC 4248	7.21	28	2008-03-08	2013-01-10	4.8	1.09	25.60	13
NGC 4258	7.21	28	2008-03-08	2013-01-10	4.8	1.09	25.60	13
NGC 4395	4.27	4	2008-03-10	2013-01-09	1.7	0.44	25.60	14
NGC 4449	3.82	6	2008-03-09	2013-01-09	4.8	0.32	25.70	15
NGC 4605	5.47	5	2008-03-13	2013-01-10	2.1	0.53	25.72	16
NGC 4736	5.08	5	2008-03-10	2013-01-09	3.9	1.19	26.23	17
NGC 4826	4.40	6	2008-03-08	2013-01-10	4.7	0.35	26.23	2
NGC 5194	8.30	8	2008-03-09	2013-01-10	3.9	0.93	26.16	18
NGC 5474	6.43	7	2008-03-13	2013-01-10	3.9	0.60	26.16	3
NGC 6503	5.27	7	2008-05-04	2012-10-15	4.3	0.70	26.16	6
NGC 6946	5.96	19	2008-05-03	2012-10-17	4.5	0.16	25.94	19
IC 2574	4.02	9	2008-03-13	2013-01-10	4.7	0.46	26.06	6

The baseline is the time from the second observation to the last observation in the selection period. The flux calibration $\nu L_\nu/L_\odot$ gives a sense of the number of counts expected from a star of a given luminosity. The depth is the LBC/ETC estimate of $SNR = 5$ for the R_c band depth of the observations in an extragalactic field (i.e. a normal sky background). References – (1) Gerke et al. 2011; (2) Jacobs et al. 2009; (3) Shappee & Stanek 2011; (4) Herrmann et al. 2008; (5) Karachentsev et al. 2004; (6) Karachentsev et al. 2003; (7) Willick et al. 1997; (8) Drozdovsky & Karachentsev 2000; (9) Verdes-Montenegro et al. 2000; (10) Theureau et al. 2007; (11) Kanbur et al. 2003; (12) Dopita et al. 2010; (13) Herrnstein et al. 1999; (14) Thim et al. 2004; (15) Annibali et al. 2008; (16) Karachentsev et al. 2006; (17) Tonry et al. 2001; (18) Poznanski et al. 2009; (19) Karachentsev et al. 2000.

the reference images. The U band photometric solution for NGC 6946 was determined using Botticella et al. (2009) for chip 2 and Sahu et al. (2006) for chip 1. The photometric solution for chip 3 was determined using overlaps between epochs with chip 2. The R_c and V solutions were found using photometry from Welch et al. (2007). The B band solutions for chips 2 and 3 were found using SINGS ancillary data (Kennicutt et al. 2003). The B band calibration for chip 1 at NGC 6946 and the R_c band of NGC 6503 were calibrated using the USNO-B1.0 catalog (Monet et al. 2003). We required the sources used for calibration from the USNO-B1.0 catalog to be detected in both epochs and have the two measurements agree to within 0.3 mag. The photometric solutions for the B and V bands of NGC 6503 were found using the HST Guide Star Catalog 2.3. IC 2574 and NGC 925 were calibrated in the B , V and R_c bands using the SINGS ancillary data (Kennicutt et al. 2003). For the present study, the U band data for IC 2574, NGC 925 and NGC 6503 remain uncalibrated. We are actively addressing calibration issues for future work. The typical photometric errors are 0.06 mag. Since we are looking for large changes in luminosity, our absolute photometry does not require a high level of

precision, although the calibrations of the latter few galaxies clearly require improvement. When we select candidates based on luminosity cuts, we correct for Galactic extinction using the estimates from Schlafly & Finkbeiner (2011).

We mask the images in two different ways. First, we create a subtraction mask that is applied before the ISIS image subtraction. On all images we apply a 9 pixel radius mask around any pixel exceeding 60,000 counts using IRAF. This removes saturated stars and most of their associated bleed trails, which are a dominant cause of erroneous variable sources. The reference image mask combines the masks of all the images used to construct it. This masking significantly improves the quality of the image subtraction and reduces the number of spurious variable sources. As discussed below, we catalog and track the individual saturated stars that lead to masked regions. However, we do lose the fainter stars that lie in the masked regions.

Unfortunately, subtractions near the edges of the masked regions are then damaged by the presence of the edge. So for candidate selection we use a “survey” mask. This second type of masking expands the subtraction masks a further 5 pixels and also masks the chip edges where image

Table 2. Field Masking Percentage Fractions

Galaxy	Chip	U	B	V	R	All
M81	1	4.0	5.9	6.8	7.5	3.2
	2	4.0	7.3	9.3	8.7	3.2
	3	3.4	7.4	8.2	5.5	2.9
	4	4.4	5.8	6.9	6.3	3.0
M82	2	10.2	13.7	15.0	11.6	6.9
M101	1	5.0	5.3	6.0	5.1	3.4
	2	4.0	4.6	5.4	5.2	2.9
	3	3.7	4.2	5.1	4.6	2.7
N628	4	5.0	5.2	5.5	3.4	2.6
	1	12.7	8.6	9.7	6.7	3.5
	2	9.0	6.6	7.7	7.2	4.5
N672	3	9.3	9.8	7.8	7.1	4.0
	2	5.6	9.3	9.9	10.0	4.4
N925	4	6.7	7.5	8.9	11.2	4.5
	2		8.6	10.6	14.9	6.3
N2403	1	4.8	5.3	6.5	4.3	3.0
	2	4.0	5.0	7.9	7.7	3.0
	3	4.1	4.7	5.6	4.6	3.0
	4	5.3	7.7	10.0	12.8	3.0
N2903	2	13.9	15.6	14.4	8.1	4.5
N3077	2	5.9	8.5	9.5	6.7	3.3
N3344	2	6.3	7.7	9.9	12.6	5.3
N3489	2	4.0	4.2	5.3	11.1	3.6
N3627	3	5.2	6.1	7.3	9.3	3.2
N3628	1	5.0	5.1	9.4	3.5	2.8
N4214	2	6.4	6.4	10.5	6.8	5.1
N4236	2	11.8	6.4	12.6	6.8	5.6
N4248	4	6.6	6.7	6.7	5.8	4.1
N4258	2	4.8	4.6	5.1	7.1	3.0
N4395	2	9.0	9.1	9.4	7.3	6.6
N4449	2	5.8	6.1	5.6	5.3	4.4
N4605	2	4.9	5.2	8.8	3.8	3.1
N4736	2	12.1	12.6	12.8	3.2	2.5
N4826	2	5.0	4.8	6.0	4.4	3.1
N5194	2	6.9	7.9	8.2	6.2	4.5
N5474	2	5.9	6.2	7.5	4.7	3.0
N6503	2		9.7	7.8	8.5	4.7
N6946	1	7.4	9.8	17.8	19.7	4.0
	2	8.5	11.7	22.1	25.8	5.3
	3	7.0	8.5	17.8	20.3	4.7
I2574	2		7.4	7.8	5.2	4.1

The percentage fraction of each pointing/field that is masked both for the individual filters and in all filters (i.e., the “logical and” of the masks). The missing *U* band entries are those lacking a *U* band photometric calibration.

centering shifts produce subtraction artifacts. To estimate the fraction of the galaxy we are surveying, we calculate the masked area. Table 2 reports the fraction of each pointing/field that is masked for both the individual filters and the fraction that is masked in all filters (i.e., the “logical and” of the masks).

4 CANDIDATE SELECTION

To search for variable and ultimately vanishing stars, we combine several approaches to target selection. We start with three lists of potential candidates. We perform PSF photometry using DAOPHOT on the reference image and

create a list of bright sources. We define a bright source as one having an observed luminosity of $\nu L_\nu \geq 10^4 L_\odot$ in any band. Second, we identify all the variable sources in our survey. The variable sources are identified by performing aperture photometry using SExtractor on the RMS image. The RMS image is the pixel by pixel root mean square (rms) average of the subtracted images formed after eliminating those with seeing FWHM above $2''.0$. Each subtracted image is convolved with a Gaussian of width, $\sigma^2 = (2''.0^2 - FWHM^2)/8 \ln(2)$, designed to give all the subtracted images a similar resolution of $2''.0$. Finally, we created a list of saturated sources that are masked in the reference image.

To remove artifacts from our source lists, we impose a cut on the flux ratio of two different apertures on the RMS image. Effectively, this cut removes SExtractor detections that are not point-like variable sources. We performed IRAF aperture photometry on the RMS image using a 4 and an 8 pixel radius aperture, F_4 and F_8 , for both our variable and bright sources. Experiments and visual inspection demonstrated that $F_4/F_8 > 0.4$ for real sources, and we reject a source that fails this test in all four filters.

We then combine the bright and variable lists, matching sources that are within 1 pixel of each other. Finally, we add the list of masked stars to create a final list of targets. ISIS light curves are then created for all targets that are not masked in the reference frame. These target lists are independently created for each of the 4 bands. For candidate selection we examine the light curves from the beginning of the survey through the observing run ending 10 January 2013. The first and last observation dates for each galaxy are reported in Table 1. We use the data taken after the January 2013 run to help determine the nature of any candidates.

Ideally, we would have an accurate magnitude for each source in the reference image which we would use to normalize the difference imaging light curves. We would then simply analyze these light curves. In practice, confusion and saturation in the reference image means that we must consider several different cases. Furthermore, whether a target is masked can change over the course of the survey. Some of the changes are caused by astrophysical phenomena, like novae. Some of the changes are caused by properties of the data such as seeing variations or the size and rotation of the diffraction patterns from bright stars. We can broadly divide the possible scenarios by whether the source is (1) never masked, (2) masked in the reference image, or (3) unmasked in the reference image but masked in some observational epochs.

4.1 Sources Unmasked in the Reference Images

The targets found on the list of bright and/or variable sources are by definition unmasked in the reference image. For each source we produce an unnormalized light curve in $\Delta\nu L_\nu(t) = \nu L_\nu(t) - \nu L_\nu(ref)$. We would also like an estimate of the normalized light curve, $\nu L_\nu(t)$, which requires an estimate of the source luminosity, $\nu L_\nu(ref)$, in the reference image. While $\Delta\nu L_\nu(t)$ suffers little from crowding or blending, there are challenges for estimating $\nu L_\nu(ref)$.

We estimate $\nu L_\nu(ref)$ in one of three ways. If a target matches a source in our full DAOPHOT catalog for the ref-

erence image, then we use this to normalize the light curve. While all bright targets have a DAOPHOT magnitude by definition, not all of the variable targets will be found as a source in the reference image. If no DAOPHOT source is found, we perform aperture photometry using IRAF on the reference image at the target location on the RMS image. If a significant flux is detected, we use this to normalize the light curve. Aperture photometry typically failed in areas of high background or near masked pixels. If aperture photometry fails, the light curve is normalized to the largest decrease in luminosity seen in the light curve since the target must be at least that bright. Essentially, we set the minimum $\Delta\nu L_\nu(t) = 0$.

Given $\Delta\nu L_\nu(t)$ and our best estimate of $\nu L_\nu(t)$ we define several broad criteria to select candidates for failed SNe. The first set of criteria performs a general search for a source that has a large decrease in luminosity, possibly vanishing by our last observation. These criteria make no assumptions about the nature of any transient associated with black hole formation. We are simply looking for a vanishing massive star. As discussed earlier, the Padua stellar models (Marigo et al. 2008) or the Groh et al. (2013) stellar models show that a luminosity limit of $\nu L_\nu \sim 10^4 L_\odot$ will capture the evolved stars expected to experience a SN that do not experience a high level of mass loss and become the stripped Wolf-Rayet stars responsible for Type Ib and Ic SN (see Figure 1). We simply calculate the change in luminosity between the first and last observation from the differential light curves. If the change in luminosity is $\nu L_\nu(t_1) - \nu L_\nu(t_N) \geq 10^4 L_\odot$, the source is considered a possible candidate. Note that this criterion is independent of $\nu L_\nu(ref)$. We also identify objects that become significantly brighter $\nu L_\nu(t_N) - \nu L_\nu(t_1) \geq 10^4 L_\odot$ and follow these sources as we would a fading possible candidate. This criteria was designed to be broad, not requiring any particular signature for a failed SN since the optical signature is uncertain. Instead we search for a source that is clearly detected at the beginning of the survey and at some point becomes undetectable for the remainder of the survey. No matter what the signature of a failed SN, the progenitor star will ultimately vanish in our bands. The brightening candidates allow us to explore our false-positive rate and will provide a sample of novae and other bright variables.

The second set of criteria address sources that become masked at some point in the survey, but are not masked in the reference image. Changes in a target's masked status can be due to astrophysical phenomena as well as changes in the data, such as small changes in the rotator angle. It is very difficult to automatically separate these two causes for a masking change. However, our multiple bands help minimize this problem. For example, if a target in the R_c band moves in and out of our masking limit with changing seeing, it is very likely this source will be unmasked in one of the bluer bands. Since we do the initial candidate selection independently in each band, sources that are occasionally masked in a band are considered a possible candidate if the target is masked at any point in the survey and is found during our last observation to have a luminosity $\nu L_\nu \leq 10^4 L_\odot$. When we match candidates between the bands, as will be described later, we examine such sources in bands where they are unmasked, if possible.

Our last set of criteria is designed to identify the failed

SN signature identified by Lovegrove & Woosley (2013) for red supergiant progenitors. While the shock breakout during a failed SN, discussed in Piro (2013), produces a brighter optical transient, it only lasts for 3–10 days and this is too short to search for given our survey cadence. Lovegrove & Woosley (2013) found that for 15 – 25 M_\odot red supergiants the envelope of the stars becomes unbound, producing a transient that lasts about ~ 1 year with a luminosity of order $L_{bol} \sim 10^6 L_\odot$ and a temperature of ~ 4000 K at peak. We can easily search for such a source by selecting all targets that have a luminosity of $\nu L_\nu \geq 10^5 L_\odot$ for between 3 months and 3 years during the survey. We impose this broad timing window to exclude objects that are always high luminosity or reach this luminosity only briefly. The luminosity limit is lower than $L_{bol} \sim 10^6 L_\odot$, because we must take into account bolometric corrections. The changes in the blue bands will be smaller given the expected temperature, so this is primarily a search in the R_c and V bands.

4.2 Saturated Stars in the Reference Images

The reference images are constructed from the best quality images of each galaxy. This means that the reference image is generally comprised of images with the smallest FWHM, leading to the maximum number of saturated stars. The absolute magnitude at saturation varies from galaxy to galaxy, ranging from roughly -9.5 to -11.5 mag in the R_c band and from roughly -10 to -12.5 mag in the U band. The sources masked in the reference image are not necessarily masked in all the survey images, either because of changes in seeing or due to actual luminosity changes of the source. For example, a star that is saturated in R_c may not be saturated in U band. For saturated stars in the reference image we simply check their fluxes in the final epoch. We search the DAOPHOT catalog of the last image within a 3 pixel radius around the location of the star and pick the brightest source as our match. We search a larger radius because the location determined for the masked star in the reference image is approximate. If the source is still saturated or bright we ignore it. However if the luminosity in the final image is $\nu L_\nu \leq 10^5 L_\odot$, the source is considered a possible candidate and is visually inspected. If no match is found, aperture photometry is performed at the location. If the source is still masked, it is considered saturated and not a candidate. If a non-zero flux is found, the source is considered a possible candidate.

4.3 Summary of Candidate Identification

To summarize, the initial target list was comprised of sources that were not identified as artifacts and satisfied one of these three criteria.

- (1) Luminous ($\nu L_\nu > 10^4 L_\odot$) in the reference image,
- (2) A source in the RMS variability image, or
- (3) Masked at some point,

in any of the four bands. Each such target was then considered a candidate if it showed either

- (1) A difference between the first and last observation of $|\Delta\nu L_\nu| > 10^4 L_\odot$,

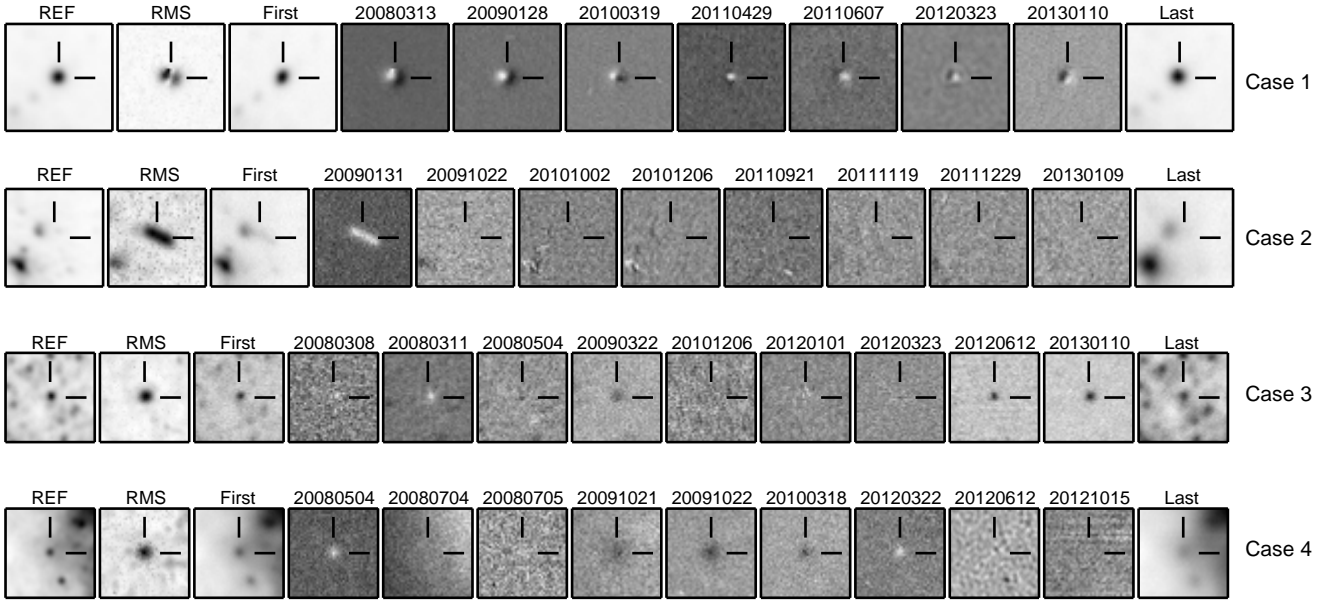


Figure 2. Four examples of sources that were selected as candidates and removed from the candidate list through visual inspection. In the subtracted images, which show the individual images minus the reference image, darker shades mean the source is dimmer than in the reference image and whiter shades mean it is brighter. For the REF, RMS, First, and Last images, the darker the source, the brighter it is. Case 1 is a bright star with “dipole” subtraction residuals. These are the most common false positives. Case 2 is an asteroid. These are relatively uncommon and are easily removed due to their motion. Case 3 and Case 4 are both variable stars that happen to be dim at the end of our selection period. In most cases they are easily removed because they continue to vary after the end of the survey period. We show the reference image, the RMS image (where the brighter the source, the more it varied over the course of the survey), the first observation, a selection of the subtracted images labeled by their epoch and, finally, the last observation. The images are 10 arcseconds on a side.

(2) $\Delta\nu L_\nu > 10^5 L_\odot$ for 3 months to 3 years during any point of the survey, or

(3) It was masked at some point in the survey but was found to be unmasked and no longer bright in the last observation.

4.4 Processing the Candidates

Once we identify possible candidates in each of the bands, we cross match the bands using a 1 pixel radius. We next compare the DAOPHOT PSF luminosity from the last observation to that found by ISIS for each band in which the source is a candidate. If in any band these measurements match to within 0.3 mag and the candidate has a luminosity in the final image above $\nu L_\nu \geq 0.25 \times 10^4 L_\odot$, then the detection and measurement are considered secure, and we eliminate the candidate. If the photometry in the final image does not meet these criteria, then the candidate is visually inspected.

At this point we were left with 11,134 candidates across all galaxies and filters. Two of the authors (JG and CSK) vi-

sually inspected all the remaining candidates. We inspected candidates that are never masked in the longest wavelength band they are found as a candidate. If a candidate is sometimes masked or masked in the reference image, and is never masked in another band, we inspected it in that band. If the candidate is unmasked in multiple bands, we inspected it at the longest wavelength band available. Often, sources masked in the R_c band are not masked in the U band. If the target is sometimes masked in all bands, we inspected the target in the longest wavelength band it was found as a candidate.

For the visual inspection, we looked at postage stamps around the source in the reference image, the last observation, the RMS image and each subtracted image in the survey. We constructed light curves and selected candidates from the survey data taken through January 2013. Data taken after this period were used to help determine if the source remained faint or was a persistently variable source. If we detect the source after January 2013 either directly in the image or through variability we declare that the source is not a failed SN and no longer a candidate.

The most common classifications of sources that did not survive as candidates are true variable stars that are clearly present after January 2013 and inconsistent subtraction of bright stars creating false candidates. Figure 2 shows 4 different examples of sources that were selected as candidates and removed through visual inspection. Case 1 (top) shows an example from NGC 5474 of the inconsistent subtraction of bright stars. Such sources are easy to identify and remove from the candidate list. Case 2 shows an asteroid in the field of NGC 628. Case 3 and Case 4 both show variable stars. Case 3 is in M101 and fades over the course of the survey selection period, but is clearly present in the last observation. Case 4 shows a variable star in NGC 6503 that does not steadily fade. It happens to be dimmer at the end of our candidate selection period in 2013, but the bright star is still visible in the last observation from 2014. This case also illustrates how poorer quality data, like the last observation NGC 6503, causes ambiguity. Many of the candidates that survived the first round of inspections were from galaxies that were less well sampled or had poorer quality data. Candidates were kept if either inspector considered it a candidate.

This first round of visual inspection resulted in a list of 235 residual candidates. Candidates that passed through the first round of visual inspections were then examined a second time using all available bands, which helps clear up most remaining ambiguities. For example, an area which is crowded in the R_c band may be much more sparse in the U band and something near the detection threshold in the V band may be a clear detection in the R_c band. This more detailed inspection of the candidates reduced the number of candidates to 14. A final round of inspections with additional data was completed adding the calibrated light curves to both aide our interpretation of the subtracted images and for detailed checks of their light curves. We were left with 4 final candidates, which we will discuss in more detail in sections 6 and 7.

In addition to selecting our failed SN candidates, our search allows us to compare the number of variable sources that had faded at the end of the selection period to those that had brightened. We would expect there to be about the same number of sources that had increased in brightness as those that had decreased in brightness and indeed this is the case. We find 3586 fading variable sources and 3514 brightening variable sources, giving a ratio of 1.02 ± 0.02 . This helps show that we are not preferentially detecting sources that fade, but instead detect variable sources that are fading and brightening with roughly equal efficiency. We also detected ~ 40 sources that met our Lovegrove-Woosley model based criteria, but all of these sources were ultimately rejected.

5 SUCCESSFUL SUPERNOVAE

We can use the successful core-collapse SNe (ccSNe) in these galaxies as tests of our approach. We processed these sources just as we would any star, basically performing a blind search for a vanishing star, as long as our last observation is taken after the SN has sufficiently faded. During our survey period there were three core-collapse SN (SN 2009hd, SN 2011dh, and SN 2012fh) and one Type Ia SN (SN 2011fe) in our

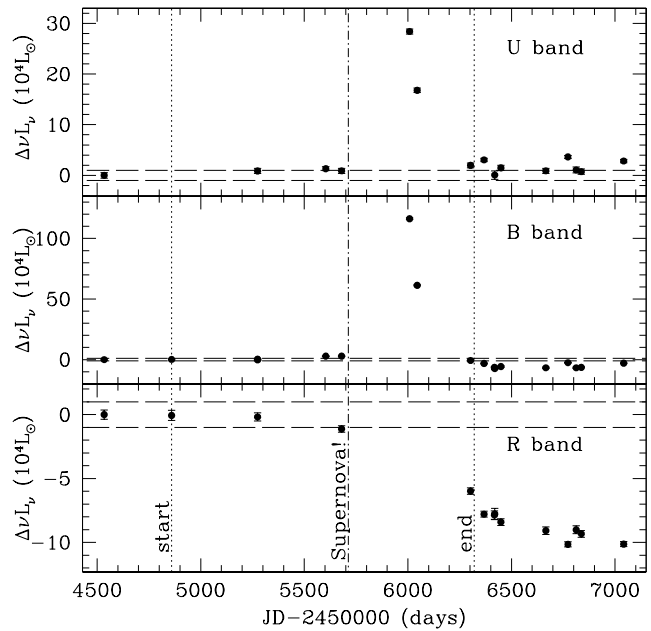


Figure 3. The U (top), B (middle) and R_c (bottom) band differential light curves for SN 2011dh in M51. For the U and B bands we show the results as originally processed, while for R_c we show a reprocessed series where the reference image included only images prior to the SN. The vertical axis is in units of $10^4 L_\odot (\nu L_\nu)$ and has been normalized to the first observation so that the luminosity difference between the first and last observations can be easily seen. Note, however, the change in luminosity scale between the U/B images showing the SN and the R_c images that do not. A change in luminosity by $10^4 L_\odot$ in either direction, marked by the horizontal lines, would lead to the source being selected as a candidate. The vertical dotted lines show the beginning and end of the candidate selection period.

sample. Here we discuss the 3 ccSNe that occurred during our search window.

The first SN that occurred during our candidate selection period was SN 2009hd in NGC 3627 (Monard 2009; Elias-Rosa et al. 2011). This SN exploded in June 2009 when we had 3 epochs of data. The SN occurred in a dusty region and because of the resulting low progenitor fluxes and the sparsity of epochs we have no useful information on the variability of the progenitor. We have 4 epochs after the explosion and during our candidate selection period, with the last observation on 28 April 2012, plus 5 additional epochs after the selection period. This source was chosen as a brightening candidate in the U , B , and V bands. In the R_c band, the source fell next to a bright star that is masked in our images. The luminosity of the SN is still brighter than the progenitor even in 2014, probably because of interactions between the SN shock and the circumstellar medium. As a result, we did not find it as a faded star. A failed SN, even with mass ejection as in Lovegrove & Woosley (2013), could not produce this bright long-term luminosity because there would be either no shock or a very weak shock. Shock driven luminosities scale as $L \propto v_s^3$ where v_s is the shock speed, so a failed SN with $v_s \sim 200$ km/s would be about $(200/4000)^3 \sim 10^{-4}$ times less luminous than a true SN with

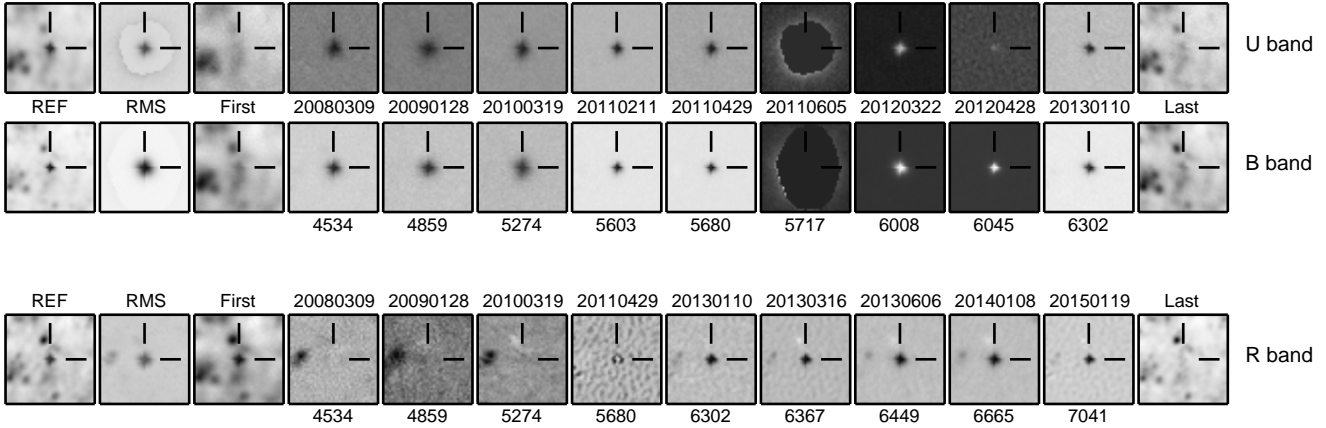


Figure 4. The top and middle rows show the U and B band images for SN 2011dh from our original candidate selection process and the bottom shows the R_c band images from our experiment creating a reference image using only observations taken prior to the SN. We show R_c band images without the SN from the candidate selection period and only select observations from afterward. The “First” observations are on 9 March 2008 and the “Last” observations shown in the U and B bands are on 10 January 2013 and on 19 January 2015 for the R_c band. The format is the same as in Figure 2.

$v_s \sim 4000$ km/s and could not sustain the luminosity of a massive evolved star.

The best test of our search algorithm is SN 2011dh in NGC 5194. This type IIb SN was discovered quickly after its May 31 explosion (Griga et al. 2011). At the time of the SN, we had 5 epochs in UBV and 4 epochs in R_c . The progenitor was easily visible and found to be variable in our LBT data, as discussed in detail in Szczygiel et al. (2012). We have 4 additional epochs during our selection period after the SN occurred. The last observation of the source in our candidate window was on 10 January 2013, one of the last observations to be included.

SN 2011dh was selected as a candidate in all four bands, although not truly based on the star vanishing. In the present data, the source was selected because of the SN surviving as a candidate in the U , V and R_c bands. In the U and B bands, the SN exceeded the “brightening” luminosity ($\Delta\nu L_\nu \geq 10^4 L_\odot$) and it was kept as a candidate in U both for brightening and matching the Lovegrove-Woosley model based criteria. It was not kept as a candidate in the B band, where it had not faded sufficiently. It would have been selected at B band had we used the next epoch in March 2013. In the R_c and V bands it was selected because it had been masked in the reference image due to the inclusion of the SN and was unmasked and not found by DAOPHOT in the final epoch (V band) or found to have significantly faded (R_c band). The inspections periodically led to a frisson of excitement when this source came up because the vanishing of the progenitor is unambiguous in any visual inspection of the later data.

As an experiment, we explored what would happen if the SN was removed from the R_c band data. We created a new reference image using images from before the SN and removed observations where the SN was masked. Figure 3

shows the differential flux light curves for the U and B bands from our original blind analysis while the R_c band light curve is from our analysis removing the SN. The progenitor began with a luminosity of $8.3 \times 10^4 L_\odot$ in the U band, $2.01 \times 10^5 L_\odot$ in the B band and $1.08 \times 10^5 L_\odot$ in the R_c band. The R_c band source is clearly fading and the source would have been considered a fading candidate during the candidate selection period. Figure 4 shows the U and B band images from our original candidate selection and select R_c band images from all survey observations. We show the RMS image (where the brighter the source, the more it varied over the course of the survey), the reference image, the first observation, the subtracted images labeled with the epoch and finally the last observation. In the U and B bands there was not enough time to fade below the luminosity of the progenitor. In the R_c band, the subtracted images show the low level of fading found by Szczygiel et al. (2012) before the SN. There is a definite signal afterwards, signifying the lack of flux from the progenitor. If we analyze this source, it is flagged as a vanishing star candidate. If we include the data later than January 2013 the signal becomes even stronger, as shown in Figure 3. This shows that our methods are valid and able to discover vanishing stars.

The final ccSN that occurred during our candidate selection was the Type Ic SN 2012fh in NGC 3344 (Nakano et al. 2012). While there are 8 epochs of observations between 04 May 2008 and 23 March 2012, there are no observations between when the SN occurred (likely 2013/06, Nakano et al. 2012) and 10 January 2013, the end of our candidate selection period. Therefore, we cannot use this SN to test our procedures.

There are 2 remaining events that are special cases. We caught the transient SN 2008S in NGC 6946 in outburst at the beginning of our survey. We do not have any pre-

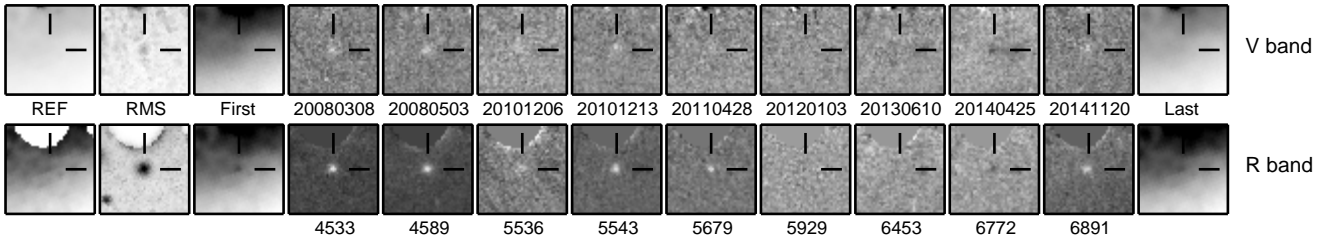


Figure 6. Selected V and R_c band observations of Candidate 2 in NGC 4248. We have 29 epochs for this galaxy in total. The “First” observation is on 8 March 2008 and the “Last” observation is on 20 November 2014. The format is the same as in Figure 2.

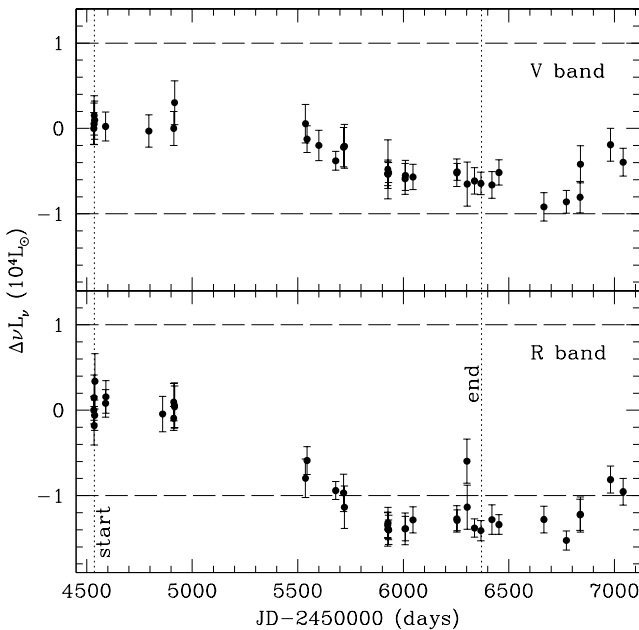


Figure 5. The V (top) and R_c (bottom) band differential light curves for Candidate 2 in NGC 4248. The vertical axis is in units of $10^4 L_\odot (\nu L_\nu)$ and has been normalized to the first observation so that the luminosity difference between the first and last observations can be easily seen. A change in luminosity by $10^4 L_\odot$ in either direction, as indicated by the horizontal lines, would lead to the source being selected as a candidate.

explosion images from this survey, as our first observation was taken 3 May 2008. Although Prieto et al. (2008b) discusses the progenitor of SN 2008S using LBT observations taken before the explosion, this data was not included in our analysis. In our survey, this source was chosen as a candidate in all 4 filters due to a decrease in luminosity of $\nu L_\nu \geq 10^4$ between the first and last observations. SN 2011fe, a Type Ia in M101 (Nugent et al. 2011), occurred in our sample during our candidate selection period. This source was selected as a candidate due to the SN explosion itself. It had not faded enough by the end of our selection

range and it will not test our methods because the progenitor is constrained to be far fainter than an evolved massive star (Li et al. 2011).

6 ULTIMATELY REJECTED CANDIDATES

Our survey produced 4 final failed SN candidates, two of which were promising, Candidates 1 and 2, and two which were more ambiguous, Candidates 3 and 4. With additional LBT data from late 2014 and early 2015 we can reject Candidates 2, 3 and 4 with reasonable confidence, with additional evidence from archival *HST* observations to support the rejection of Candidate 3. This leaves Candidate 1 as the only current candidate. We discuss the ultimately rejected Candidates 2, 3 and 4 to illustrate the selection process.

These three sources all showed decreases in luminosity between the first and last observation of $\nu L_\nu \geq 10^4 L_\odot$. Candidate 2 was considered a good candidate, with a clearly visible source at the start of the survey that faded to become undetected. Candidates 3 and 4 were more ambiguous, as they are dimmer sources next to brighter stars in galaxies with poorer data. One candidate is next to a masked region of a bright star and the other is a red source that is blended with a brighter star. Here we explore why these 3 candidates were selected, then removed, from candidacy.

For a vanished star, the change in luminosity we measure between our first and last observations during our candidate selection period is exactly equal to the total luminosity of the star if it has vanished. Since two of our sources are in crowded regions, these differential magnitudes will be a more accurate measure of the SED of a star which has actually vanished than direct photometry on the initial observations.

6.1 Former Candidate 2

This candidate was found in NGC 4248, a dwarf companion galaxy to NGC 4258, at RA 12:17:50.56 and Dec +47:24:27.65. It was selected as a fading candidate in the R_c band. The source was also detected in the V band but not in the U or B bands. Figure 5 shows the R_c and V

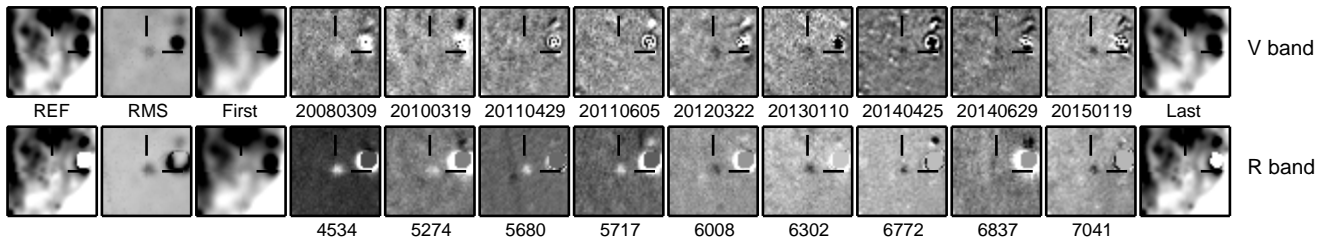


Figure 8. Selected V and R_c band observations for Candidate 3 in NGC 5194. The “First” observation is on 9 March 2008 and the “Last” observation shown is from 19 January 2015. The format is the same as in Figure 2.

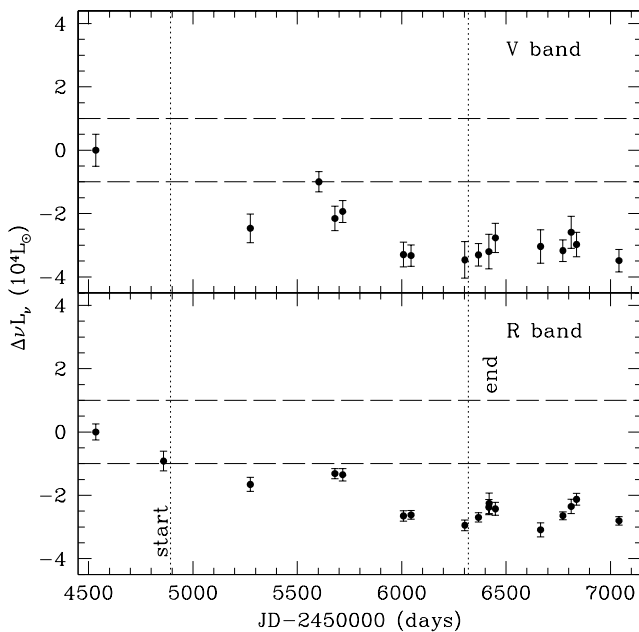


Figure 7. The V (top) and R_c (bottom) band differential light curves for Candidate 3 in NGC 5194. The star is on the edge of a masked region, leading to poorer than usual photometry. The format is the same as in Figure 5.

band differential light curves for this candidate. We see in both bands that the source begins the survey at a relatively constant luminosity for a year. We measured the luminosity decrease during our survey period to be $1.3 \times 10^4 L_\odot$ in the R_c band and find an apparent magnitude of $R_c \simeq 23.06$ mag. In the V band we measure a luminosity decrease of $0.7 \times 10^4 L_\odot$ and an apparent magnitude of $V \simeq 24.19$, giving a $V - R$ color of $\simeq 1.13$ mag. Figure 6 shows select observations from the 28 total epochs for this galaxy. The candidate is no longer visible after 28 April 2011, about when the luminosity decrease crossed our threshold to consider the source a candidate in the R_c band. Observations taken with the LBT on 20 November 2014 and 19 January

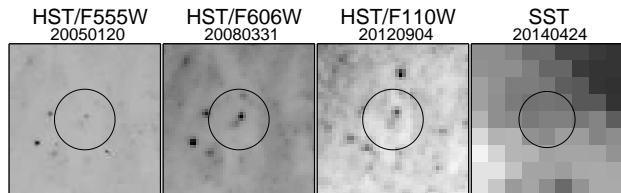


Figure 9. Selected archival observations for Candidate 3 in NGC 5194. From left to right the panels show the $F555W$ *HST* observation from 2005 January 04, the $F606W$ observation from 2008 March 31, the $F110W$ observation from 2012 September 4 and an example $3.6\mu\text{m}$ *SST* observation. We can see in the *SST* image that there is mid-IR emission in the region, but cannot resolve a particular source. The archival images are labeled with the date of the observation. The circle marks the Candidate location and has a 1 arcsecond radius. The images are 5 arcseconds on a side.

2015 show the source, after almost 3 years below our detection limit, became visible again. This reappearance means this variable star is not a failed SN.

While there are no *HST* archival observations of Candidate 2, there are IRAC *SST* observations from 2007 (Program: 40204, PI: Kennicutt) and 2010 (Program: 61008, PI: Freedman). There is no source visible at the location of Candidate 2 in either of these epochs. For the $3.6\mu\text{m}$ ($4.5\mu\text{m}$) data we calculate a 3σ flux limits of 0.0411 ± 0.0005 mJy (0.029 ± 0.001 mJy), which are too weak to constrain the mid-IR luminosity.

6.2 Former Candidate 3

The candidate found in NGC 5194 at RA 13:29:51.01 and Dec +47:11:26.85 was difficult to classify given its location and magnitude. It fell on the edge of a masked region caused by a bright star in both the V and R_c bands. The source was selected as a candidate due to fading in the R_c band. In addition to being next to a masked bright star, this candidate was also difficult to characterize because it is relatively faint.

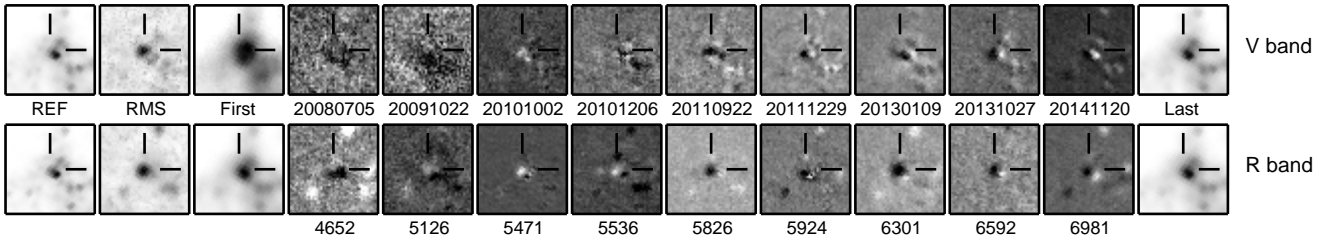


Figure 11. Selected V and R_c band observations for Candidate 4 in NGC 672. The “First” observation is on 5 July 2008 and the “Last” observation shown is from 20 November 2014. The format is the same as in Figure 2.

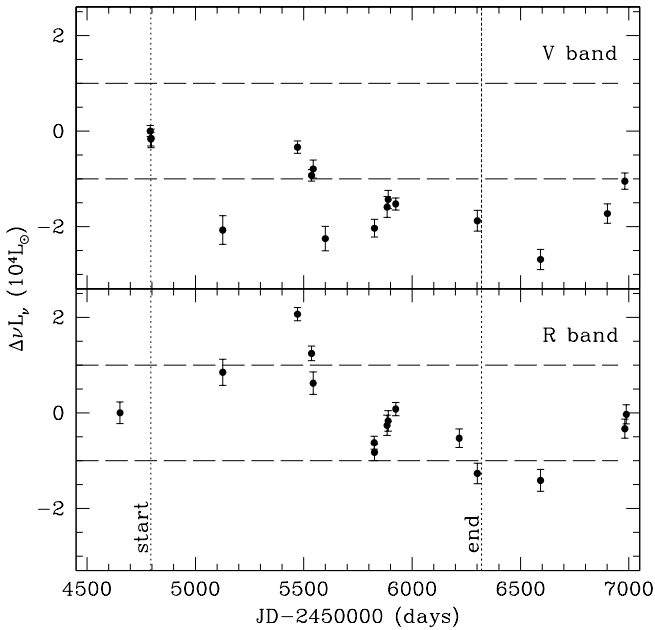


Figure 10. The V (top) and R_c (bottom) differential light curves for Candidate 4 in NGC 672. The format is the same as in Figure 5.

We reduced the amount of masking used for a nearby bright star to improve the results. The source had $R_c \simeq 22.66$ mag with a luminosity decrease of $\nu L_\nu = 2.6 \times 10^4 L_\odot$. We find a luminosity decrease of $3.1 \times 10^4 L_\odot$ in the V band and $V \simeq 22.81$ mag. The candidate was not detected in the U and B bands and no variability was seen in those bands. Figure 7 shows the V and R_c band light curves for this candidate.

The R_c band light curve shows a brightening near the end of the survey that appears to be caused by contamination from the neighboring star due to poorer observing conditions. The brightening in the V band during the last epoch, which was taken during good conditions, is also likely caused by edge effects from the masked star. No brightening is obvious in the raw images. Figure 8 shows selected

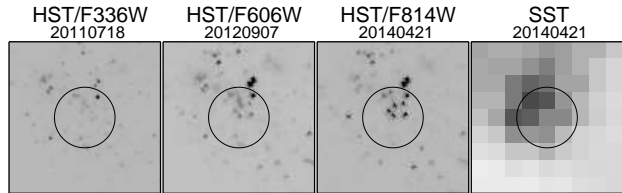


Figure 12. Archival observations Candidate 4. This figure shows the $F336W$ HST observation from 2011 July 18, the $F606W$ and $F814W$ HST observations from 2012 September 9 and the $3.6\mu\text{m}$ SST observation. The archival images are labeled with the date of the observation. The circle marks the Candidate location and has a 1 arcsecond radius. The images are 5 arcseconds on a side.

observations of this candidate. This source seems to have increased its brightness on 29 June 2014 and decreased again in the last observation on 19 January 2015. This clear variability is cause to remove this as a candidate. The archival HST observations also support eliminating this candidate.

There are archival data from both HST and SST at multiple epochs. The HST observations are available for many epochs and filters, so we only discuss select observations from the more standard, wide-field filters. We correct the astrometric solution to match our LBT reference image and find Candidate 3 corresponds to a pair of sources in the HST observations. Figure 9 shows example HST observations and an example SST observation. In January 2005 observations were taken with ACS (Program: 10452, PI: Beckwith) in the $F555W$ and $F814W$ filters. Star 1, the upper star of the two, is at RA 13:29:51.00 and Dec +47:11:26.95 and Star 2 is at RA 13:29:51.02 and Dec +47:11:26.72. Star 1 has $V=22.98 \pm 0.02$ and $I=20.93 \pm 0.01$ and the Star 2 has $V=23.92 \pm 0.03$ $I=23.18 \pm 0.02$ using DOLPHOT and correcting for galactic extinction. Observations were taken on 2008 March 31 with WFPC2 (Program: 11229, PI: Meixner) in the $F606W$ and $F814W$ filters. In these observations, we find Star 1 has $V=22.25 \pm 0.01$ mag and $I=20.44 \pm 0.01$ mag while Star 2 has $V=23.06 \pm 0.02$ mag and $I=22.98 \pm 0.06$.

Both stars appear to have brightened between 2005 and 2008.

The most recent observation, a *F110W* WFC3 IR image, was obtained on 2012 September 04 (Program: 12490, PI: Koda). This falls on the epoch between when the candidate had faded below our threshold in the R_c band and the end of our candidate selection period. We find a Vega *F110W* magnitude using aperture photometry of 20.79 ± 0.01 mag for the top source and 22.00 ± 0.02 mag for the bottom source. Both sources are also clearly visible in *F673N* and *F689M* images (Program: 12762, PI: Kuntz) taken on 2012 April 10. It is difficult to directly compare to the previous observations because of the filter differences. However, we would expect one of these stars to no longer be detected if it was a failed SN. Therefore this observation supports eliminating this candidate. Since the last observation was obtained soon after the star met our selection criteria and well before the end of our survey period, new observations would be helpful to confirm its elimination.

There are 16 epochs of IRAC data taken over 10 years (Program: 159, PI: Kennicutt; Program: 30494, PI: Sugeran; Program: 40010, PI: Meixner; Program: 70207, PI: Helou; Program: 10136 and 90240, PI: Kasliwal): 2 epochs in 2004, one in 2006 and 2007, 2 in 2008, 10 in 2011, 6 in 2012 and 2 in 2013 and 2014. There is no source visible in any observation or any detectable variability. We calculate 3σ upper limits on the source flux of $0.182 \pm .003$ mJy at $3.6\mu\text{m}$ and $0.128 \pm .003$ mJy at $4.5\mu\text{m}$, which are not constraining in terms of the mid-IR luminosity.

6.3 Former Candidate 4

The final former candidate was found in NGC 672 at RA 01:47:48.90 and Dec +27:25:28.82. This source was selected as a fading candidate in the V and R_c bands. Candidate 4 is not detected in the U or B bands and is blended with a brighter source in the V and R_c bands. Figure 10 shows the V and R_c band light curves for this candidate. We measure an R_c band luminosity decrease of $1.3 \times 10^4 L_\odot$ and an initial magnitude of $R_c \simeq 23.06$ mag. The V band decreases in luminosity by $2.2 \times 10^4 L_\odot$, giving an initial magnitude of $V \simeq 22.89$ mag. This source stayed undetected and within our criteria for candidacy for almost 2 years before LBT observations on 20 and 27 November 2014 show the source brightening, giving us solid grounds to reject it. Figure 11 shows selected observations. This source also shows the difficulties and ambiguities that can arise in areas where the image subtraction is less clean.

There are past observations of this source available from both *HST* and *SST*. The *HST* observations are in the *F336W* filter from 2011 September 7 (Program: 12229, PI: Smith) and in the *F606W* and *F814W* filters from 2012 July 18 (Program: 12546, PI: Tully). After matching the astrometry of the *HST* observations to our LBT astrometry, we find no source in the *F336W* data. There is, however, a corresponding source in the *F606W* and *F814W* filters. Using DOLPHOT to perform photometry and convert to Johnson filters and correcting for galactic extinction, we find Candidate 4 has 23.39 ± 0.01 mag in the V band and 21.34 ± 0.01 mag in the I band. Figure 12 shows the *F336W* and *F606W* observations and an example $3.6\mu\text{m}$ *SST* observation. There are archival IRAC *SST* observations for Candidate 4 taken in

2007 (Program: 40204, PI: Kennicutt) and 2014 (Program: 10136, PI: Kasliwal). This source is part of a star cluster and shows no variability in the *SST* data. The 2007 and 2014 luminosities agree within the errors at 0.145 ± 0.007 mJy at $3.6\mu\text{m}$ and 0.106 ± 0.005 mJy at $4.5\mu\text{m}$.

7 THE REMAINING CANDIDATE

Our survey period with 3 ccSNe resulted in one final failed SN candidate. This candidate shows a decrease in luminosity between the first and last observation of $\nu L_\nu \geq 10^4 L_\odot$ (see Figure 1). Candidate 1 was observed to have a relatively stable luminosity for two epochs before it experienced an outburst and then faded. Archival *HST* observations show a clear source before the outburst. Archival *SST* data show that a long, slow mid-IR transient is associated with the source but the resolution makes it impossible to securely identify our source.

The candidate was found in NGC 6946 at RA 20:35:27.56 and Dec +60:08:08.29. This candidate was first observed in May 2008 and then experienced an outburst in March 2009, after which it was no longer detected. The source was near a chip boundary and so was sometimes missed due to pointing variations, particularly in the first few years. As a result, there are some epochs where we have V band data but not necessarily R_c band or B band. It was selected as a candidate in the V and R_c bands due to a large luminosity decrease. With better sampling, this would have met our Lovegrove-Woosley model based criteria. The source's outburst caused one epoch in the V band to become masked. We reprocessed this observation so that the source was no longer masked. In the discussion below, all luminosities and magnitudes are corrected for the significant Galactic extinction of $E(B - V) = 0.30$. We measured a luminosity decrease in the R_c band of $5.2 \times 10^4 L_\odot$ and an apparent magnitude of $R_c \simeq 21.19$ mag. The V band luminosity decrease is $3.8 \times 10^4 L_\odot$ giving an initial V band apparent magnitude of $V \simeq 21.87$ mag. We estimate a $V - R$ color of $\simeq 0.68$ mag. Direct measurements of the initial magnitude of the candidate using DAOPHOT matches these values to ~ 0.1 mag.

There is no source detected in the initial U band observations and we find an apparent magnitude upper limit of 22.28 ± 0.4 mag. A U band source with 20.0 ± 0.1 mag is visible in the $1''.9$ seeing observation that corresponds to the peak brightness in V and R_c bands. The candidate was detected in November 2008 and March 2009 in the B band. The difference between the first and last B band observations shows the source had an initial magnitude of 23.55 ± 0.03 mag. While the source increases to 22.30 ± 0.04 on 25 November 2008, it is unfortunately off the chip during the observation where the V and R_c bands peaked.

Figure 13 shows the B , V and R_c light curves along with archival *Spitzer Space Telescope* $3.6\mu\text{m}$ and $4.5\mu\text{m}$ light curves that will be discussed later. We can see a source that is detected in two epochs at the beginning of the survey. In the R_c band, we observed the source on two successive nights, 3/4 May 2008 (the light curve points overlap in Figure 13). NGC 6946 was also observed in the V band on 4 May 2008 with data quality just outside our analysis criteria. We include this observation as an open point in the light

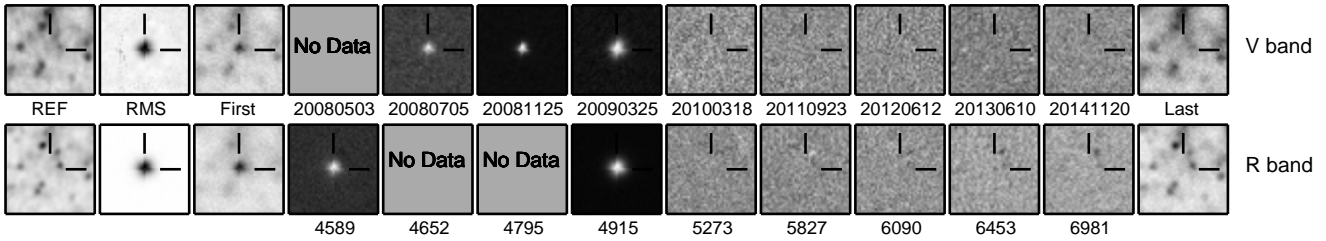


Figure 14. Select V and R_c band observations for Candidate 1 in NGC 6946. We have 19 epochs for this galaxy and do not show them all. The selected observations give a clear picture of the source’s variability. The “First” observation in the V band (R_c band) is on 5 July 2008 (3 May 2008) and the “Last” observation is on 20 November 2014. The format is the same as in Figure 2.

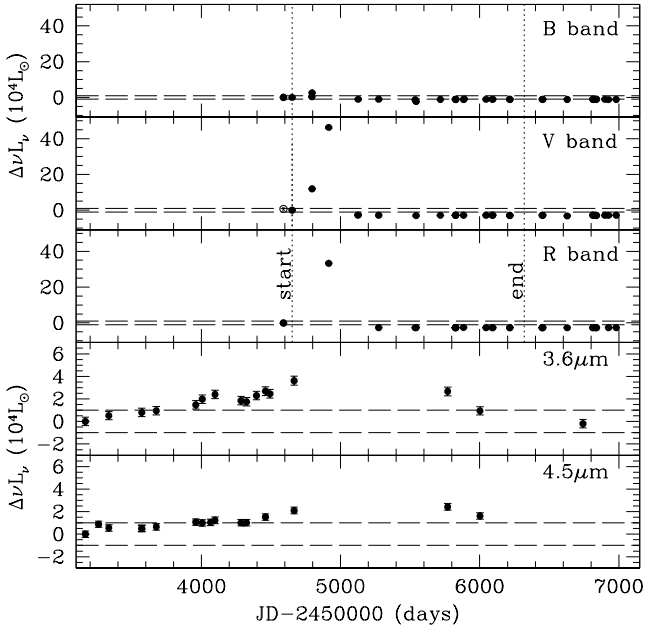


Figure 13. The B , V and R_c band differential light curves for Candidate 1 in NGC 6946. The open circle in the V band light curve was an observation that fell just outside our quality criteria that was later added as a check on the measurements. The vertical axis is in units of $10^4 L_\odot (\nu L_\nu)$ and has been normalized to the first observation so that the luminosity difference between the first and last observations can be easily seen. A change in luminosity by $10^4 L_\odot$ in either direction, as indicated by the horizontal lines, would lead to the source being selected as a candidate. The bottom two panels are the $3.6\mu\text{m}$ and $4.5\mu\text{m}$ SST archival light curves normalized to the first epoch and on a different y-axis scale.

curve and used this for our measurement of initial luminosity so that it could be compared to the R band on that same date. We measured the differential flux with simple aperture photometry as a comparison to the $ISIS$ estimates and found good agreement.

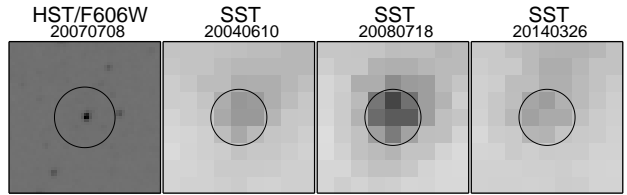


Figure 15. Archival observations of Candidate 1. The $F606W$ HST observation and the first, brightest and last $3.6\mu\text{m}$ SST observations. The archival images are labeled with the date of the observation. The circle marks the Candidate location and has a 1 arcsecond radius. The images are 5 arcseconds on a side.

The peak brightness we observe is on 25 March 2009 for both the V and R_c bands. We measure $V \simeq 18.17$ mag ($\nu L_\nu = 1.15 \times 10^6 L_\odot$) and $R_c \simeq 17.58$ mag ($\nu L_\nu = 14.34 \times 10^6 L_\odot$). After this peak, the source was not detected in any band for the remainder of our survey, with the last observation for this galaxy on 20 November 2014. Figure 14 shows select observations for both the V and R_c bands. The candidate is clearly detected in the first epoch, experiences an outburst and is not visible on or after 20 October 2009.

We found no other references to this outburst. There is a cataloged GALEX UV source close to its position, however there is also a 21.71 mag U band source within 4 arcseconds from our candidate that is likely the GALEX source. The detection of the candidate two nights in a row at a relatively unchanged luminosity in May 2008 shows that the source was present and relatively stable at the start of the survey. If this outburst was a nova or some other type of stellar variability, we expect that the star would not have been seen earlier, never fully disappeared, or should have returned. Based on the LBT data, this is a promising candidate.

There are archival observations of this source from both HST and the SST and Candidate 1 is easily identified in the observations from both telescopes. There is a single epoch of HST data from 8 July 2007 in the $F606W$ and $F814W$ WFPC2 filters (Program: 11229, PI:Meixner). Us-

ing the DOLPHOT software package (Dolphin 2002) to perform photometry and convert to Vega magnitudes and correcting for Galactic extinction, we find Candidate 1 magnitudes of 22.15 ± 0.01 in the V band and 20.28 ± 0.01 mag in the I band. There are 16 IRAC observations at $3.6\mu\text{m}$ and at $4.5\mu\text{m}$ (Program:159, PI: Kennicutt; Program: 3248, 20256 and 30292, PI: Meikle; Program: 30494, PI: Sugerman; Program: 40619, PI: Kotak; Program: 40010, PI: Meixner; Program: 80015, PI: Kochanek; Program: 10136, PI: Kasliwal). We performed image subtraction on these observations using the same procedures as for our LBT data and produced the light curves shown in Figure 13 with our LBT light curves.

Unlike the quick optical brightness decrease seen after the outburst, the increase and decrease of brightness in the mid-IR is very slow and continuous through the last observation at $3.6\mu\text{m}$ on 2014 March 26. Unfortunately, there is a gap in the mid-IR data when we see the outburst in the optical and the date and shape of the mid-IR peak are unknown. Figure 15 shows the *F606W* *HST* image and 3 of the $3.6\mu\text{m}$ *SST* observations (first, brightest and last). The archival images are labeled with the date of the observation. While there is some luminosity visible in the area of the source in the *SST* observations after it has vanished in the LBT data, and Candidate 1 could be a dusty stellar transient, it is part of some extended emission and the resolution is insufficient to securely detect the individual source seen in the LBT and *HST* observations. It could also still be fading in the *SST* bands. Additional observations, by both *SST* and *HST* are needed to determine the nature of this candidate since its outburst. We conclude that Candidate 1 is a viable candidate for a failed SN.

We fit the HST, LBT (including the U band upper limit) and SST data from near 8 July 2007, where we measure $[3.6]=17.51 \pm 0.05$ mag and $[4.5]=17.24 \pm 0.05$, using Solar metallicity Castelli & Kurucz (2004) model atmospheres obscured by circumstellar silicate dust, and using DUSTY (Ivezic et al. 1999; Elitzur & Ivezić 2001) to model the radiation transport. We assumed 10% photometric errors to compensate for mixing data from modestly different dates. If we include no circumstellar dust we find $L_* \simeq 10^{5.25 \pm 0.02} L_\odot$ and $T_* \simeq 3600 \pm 200$ K (nominally at 90% confidence) but with a best fit of $\chi^2 = 40.5$ for 7 degrees of freedom. If we include the dust, we find $L_* \simeq 10^{5.11 \pm 0.08} L_\odot$ and $T_* \simeq 4700 \pm 800$ K with $\log \tau_V \simeq 0.4_{-0.2}^{+0.1}$ of dust. The models with dust fit the data well, with $\chi^2 = 8.1$ for 6 degrees of freedom. If we map either of these models onto the end points of the Solar metallicity PARSEC isochrones (Bressan et al. 2012), they correspond to roughly $18M_\odot \lesssim M_* \lesssim 25M_\odot$ stars with the cooler, no dust models better matching the very end points of the isochrones. Thus, Candidate 1 appears to have properties that put it almost exactly in the mass range corresponding to the red supergiant problem.

8 LIMITS ON THE RATE OF FAILED SNE

If the rate of core collapses in the sample is r and the failed fraction is f , then the expected number of ccSNe and failed SNe are $N_{SN} = r(1-f)t_{SN}$ and $N_{FSN} = rft_{FSN}$, where t_{SN} is the period over which we search for SNe and t_{FSN} is the failed SNe candidate selection period. The two sur-

vey times t_{SN} and t_{FSN} need not be the same because the SN surveys of these galaxies are not solely dependent on the LBT data. To determine the constraints on the failed fraction, we assume ideal detection efficiency and use Poisson probability distributions and marginalize over the core-collapse rate r . Taking a Bayesian approach and using a logarithmic prior of $P(r) \propto (1/r)$ for the rate and a uniform prior $P(f) \propto \text{constant}$ for the failed fraction, we find the probability of getting a fraction, f , of failed SNe is proportional to,

$$P(f) \propto (1-f)^{N_{SN}} f^{N_{FSN}} (f(t_{FSN} - t_{SN}) + t_{SN})^{(-N_{SN} - N_{FSN})}, \quad (1)$$

where N_{SN} and N_{FSN} are the observed number of ccSNe and failed SNe, respectively. If we use a uniform prior $P(r) \propto \text{constant}$, we find the probability is proportional to

$$P(f) \propto (1-f)^{N_{SN}} f^{N_{FSN}} (f(t_{FSN} - t_{SN}) + t_{SN})^{(-1 - N_{SN} - N_{FSN})}. \quad (2)$$

We have dropped constant terms and the normalizations of the expressions can be found by requiring $\int_0^1 P(f) df \equiv 1$. There are explicit expressions in terms of hypergeometric functions, but they are not illuminating. The difference in the priors appears as a change in the exponent of the third term. If we set the survey times to be identical, the resulting binomial distribution, $P(f) \propto (1-f)^{N_{SN}} f^{N_{FSN}}$, does not depend on the prior on r . To constrain the fraction of failed SNe, we must choose a SN survey period, t_{SN} , with N_{SN} known ccSNe, and a failed SN survey period, t_{FSN} , with N_{FSN} failed SN candidates. To summarize, the number of ccSNe constrains $r(1-f)$, while the number of failed SNe constrains rf and by marginalizing over r , we obtain the constraint on f .

We could estimate $\langle N_{SN} \rangle$ from the historical record in the Sternberg Astronomical Institute supernova catalog. The sample galaxies had 26 probable ccSNe since 1900 along with 4 Type Ia SNe (Tsvetkov et al. 2004). If we calculate the typical rate using the time period from 1 January 2000 to 1 January 2014 there are 12 ccSNe ($t_{SN} = 14.0$, $N_{SN} = 12$), implying a rate of $r_{ccSN} = 1.01 \text{ year}^{-1}$ with a 90% confidence range of $0.55 < r_{ccSN} < 1.39$. If we go back to 1 January 1970, there were 18 ccSNe ($t_{SN} = 44.0$, $N_{SN} = 18$), implying a rate of $r_{ccSN} = 0.41$ and a 90% confidence range of $0.28 < r_{ccSN} < 0.61$, although it is also clear that the samples are almost certainly becoming incomplete on these longer baselines. However, we know we did not miss any new SNe during our survey. The survey data that is analyzed in this work is from the beginning of the survey in 2008 until the end of 2013. As discussed previously, there were 3 ccSNe during our candidate selection period ($t_{SN} = 4.0$, $N_{SN} = 3$). There was an additional ccSN between the candidate selection period and the end of 2013, the type II-P SN 2013ej in NGC 628 in July 2013 (Valenti et al. 2013). This gives a total of 4 ccSNe ($t_{SN} = 5.0$, $N_{SN} = 4$) and a rate during the overall survey of $r_{ccSN} = 0.80 \text{ year}^{-1}$, which is consistent with the recent historical record. We will use this case as our fiducial example.

For the failed SNe, we use the time from the second epoch to the last observation of our candidate selection period to find a galaxy-averaged baseline of $t_{FSN} = 4.0$ yrs. We use the second observation to begin our baseline because

Table 3. Fraction of Failed SN

t_{SN} (years)	# SN N_{SN}	# Failed SN N_{FSN}	Upper Limit		Range		Median	
			log	const	log	const	log	const
14.0	12	0	0.345	0.373				
24.0	18	0	0.462	0.522				
4.0	3	0	0.438	0.438				
5.0	4	0	0.404	0.413				
5.0	4	1	0.550	0.558	0.073 - 0.620	0.075 - 0.627	0.296	0.303

The upper limits and ranges are at a 90% confidence level. The columns labeled “log” have a logarithmic prior of $(1/r)$ on the unknown core-collapse rate while those labeled “const” have a uniform prior.

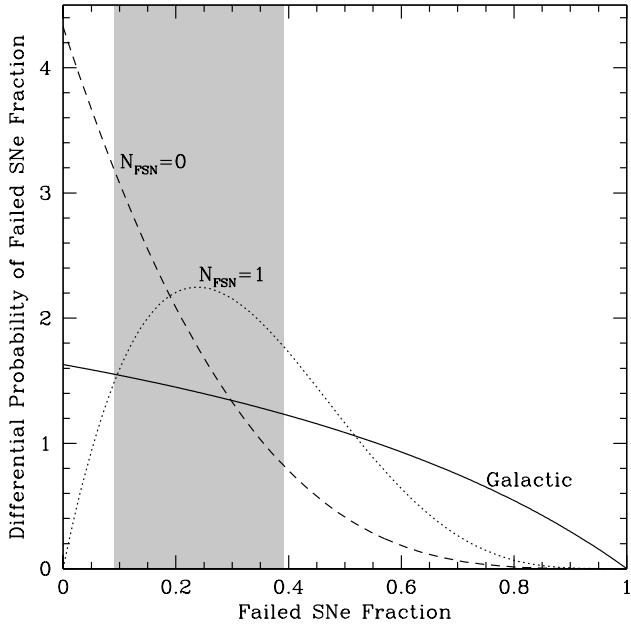


Figure 16. Probability dP/df for the fraction of ccSNe that are failed SNe if $N_{FSN} = 0$ (dashed) or 1 (dotted) failed SN are found in our sample. The solid line shows the constraints from combining the historical Galactic SN rate with the non-detection of neutrinos from a Galactic ccSN (Adams et al. 2013). Horiuchi et al. (2011) suggests $f \lesssim 0.5$ given the comparison between the SN rate and the star formation rate. The red supergiant problem is solved if $f \sim 0.2 - 0.3$ and the black hole mass function suggests $0.092 < f < 0.39$ (Kochanek 2014b) as shown by the shaded region.

we require the star to be observed for two epochs before it fades to eliminate the possibility of a false-positive caused by a nova in the first epoch. If we include the first epoch, the average baseline is 4.6 ± 0.3 years. Here we simply use the average of the survey periods for each galaxy. While there is some spread (1.7–4.8 years), how we do the average is a negligible source of uncertainty. The average masked fraction for the galaxies is $m = (3.9 \pm 1.1)\%$ which we can view as a reduction in our effective survey time, $t_{FSN} \rightarrow (1 - m)t_{FSN}$. However, we monitor saturated stars that are masked, effectively reducing the masked fraction, and the uncertainties introduced by the small masked fraction are negligible compared to our present statistical uncertainties and will be

ignored. The primary systematic uncertainty is the fraction of failed SNe we would miss because the star is heavily obscured by interstellar dust. This will be empirically explored by our ability to recover heavily extinguished SN progenitors like that of SN 2009hd.

In §7 we were left with one possible candidate failed SN. Further monitoring and new *HST* observations should clarify its status, but for now we consider the cases of $N_{FSN} = 0$ and 1. Table 3 displays the resulting constraints on the fraction f of massive stars that experience a failed SN. We calculate the limits using both a logarithmic prior of $P(r) \propto (1/r)$ (columns labeled “log”) and a uniform prior $P(f) \propto \text{constant}$ (columns labeled “const”) for the underlying core-collapse rate r . For simplicity, we first consider the $N_{FSN} = 0$ case, which occurs if the remaining candidate is ruled out. For our fiducial case ($t_{SN} = 5.0$, $N_{SN} = 4$) this leads to a (one-sided) 90% confidence upper limit of $f \leq 0.40(0.41)$ for the logarithmic (uniform) prior on r . Changing the assumed supernova survey period shifts the limits by roughly 10%, as shown in Table 3. With $N_{FSN} = 1$ the (one-sided) 90% confidence upper limit rises to $f \leq 0.55(0.50)$. Of course, with a detection we would really have a measurement, and for $N_{FSN} = 1$, the median fraction is $f \simeq 0.30$, with symmetric 90% confidence limits of $0.07 \leq f \leq 0.62$. Figure 16 shows the differential probability for the failed SNe fraction f for both of these cases.

9 DISCUSSION

This initial survey suggests several improvements for our next analysis. First, we plan to revise the masking procedure. The physical masking of the images before subtraction for reasons other than CCD defects needs to be reduced or removed entirely, with masking of saturated regions taking place after image subtraction to reduce the number of false positive detections near the edges of masked regions. One option to improve our candidate selection is to require the candidate to be securely detected for a longer period. There would be no constraints on the variability of the source since the behaviors of core-collapse progenitors are not well understood. This change would ensure we would be able to characterize any candidate reasonably well and further ensure that we were not catching the end of a nova or outburst event. The main improvement to future limits from this survey will come from an increased time baseline and SN sample. We already have an additional two years that

can be added to our survey selection period and an additional ccSN (SN 2014bc in NGC 4258; Smartt et al. 2014).

Aside from our approach, the only other prospect of detecting a failed SN is to observe neutrinos or gravitational waves from a core collapse in our Galaxy. This would have the advantage of directly probing the collapse to a black hole, but the disadvantage of a very low rate. If the Galactic SN rate is one every 50-100 years, and the failed SN fraction is $f = 0.3$, there is a failed SN in the Galaxy only once every 150 to 300 years. Adams et al. (2013) combined the observed SN rate of the galaxy with the absence of any neutrino detections (Alexeyev & Alexeyeva 2002; Ikeda et al. 2007) of a failed SN over the last ~ 3 decades to estimate that $f \leq 0.69$ at 90% confidence. Figure 16 shows how these constraints compare to those in this work. Our much larger sample of massive stars has much more power in constraining this rare phenomenon.

Other attempts to estimate the failed SNe fraction come from cosmic measurements. The non-detection of the diffuse SN background gives an upper limit of $f \leq 0.50 - 0.75$ (Lien et al. 2010). Comparing massive star formation rates to SNe rates along with the lack of a detection of a diffuse neutrino background from SNe, Hopkins & Beacom (2006) estimates that the fractional failed SN rate cannot much exceed $f = 0.5$. Horiuchi et al. (2011, also see 2014), finds a discrepancy between the cosmic SNR and the massive star formation rate which allows for a fractional failed SN rate up to ~ 0.5 (but see Botticella et al. 2012). Our limits are consistent with these estimates. The black hole mass function can be explained by a failed SN rate of $0.09 \leq f \leq 0.39$ (Kochanek 2014b) and such failure rates are consistent with studies of the “explodability” of massive stars (O’Connor & Ott 2011; Ugliano et al. 2012; Pejcha & Thompson 2014).

While the primary goal of this survey is to better understand the fates of massive stars, it enables a broad range of other scientific explorations. For example, we should be able to obtain *UBVR* photometry of all future ccSN progenitors in these galaxies. Our sensitivity in searching for the progenitor of a particular SN, where we know exactly where to conduct the search, will be considerably better than in the search for failed SNe. We estimate that we should be able to measure the properties of almost all SN progenitors because, in this case, we can compare all the stacked data prior to the explosion to as many epochs as needed once the supernova has faded rather than needing to follow the evolution of the progenitor luminosity. This can be seen in the high signal-to-noise detection of the progenitor of SN 2011dh (see Figures 3 and 4). The data also open a new field, progenitor variability, whether due to stellar activity or binarity (ellipsoidal variations or eclipses). This was demonstrated in Szczygieł et al. (2012), where we used LBT to determine the variability of the progenitor of SN 2011dh. The data are also being used to identify LBVs (Grammer et al. 2015) and to help characterize dusty evolved stars similar to η Carina or IRC+10420 (Khan et al. 2014).

Our cadence and long baseline makes this survey ideal of studying long-term variables such as Cepheids. We have completed Cepheid studies for M81 and NGC 4258, determining the distances to these galaxies and exploring the dependence of Cepheid brightness on composition (Gerke et al. 2011; Fausnaugh et al. 2014). Our large field

of view and long baseline allows us to identify Cepheids throughout the galaxy over a range of metallicities and periods $P \gtrsim 10$ days. Other possibilities include the study of the long term variability of a large population of red supergiants and searches for massive eclipsing binaries. For example, Prieto et al. (2008a) presents the discovery of an eclipsing binary in the Dwarf Galaxy Holmberg IX. Finally, this survey can also be utilized to search for other rare phenomena that produce an optical signature, such as stellar mergers (see Kochanek et al. 2014).

We should note the LBT/LBC is the best telescope/instrument for this survey. The wider field of view of Hyper Suprime-Cam on Subaru is only important for M31 and M33, but the binocular mode matters more for all other galaxies. HST could carry out the survey to a distance of 30 Mpc, but the costs would exceed even the scope of an HST Legacy Program. LSST could carry out a similar study in the South, but it would require a dedicated sub-survey (the standard exposures are far too shallow) and would have a galaxy sample with a lower ccSN rate. Moreover, if LSST starts science observations in 2022 as scheduled, it would have a data set comparable to that from our LBT survey, which is currently planned to continue till 2017, in about 2035. The most promising possible extension to this survey would be with WFIRST, although the lack of bluer optical bands will limit the characterization of the stars.

10 CONCLUSIONS

We have analyzed the first 4 years ($t_{FSN} = 4.0$) of the LBT search for failed SNe. We observed 27 nearby galaxies in the U_{spec} , B , V , and R bands multiple times a year to monitor $\sim 10^6$ red supergiants. We analyzed many target sources in our survey and are left with 1 final failed SN candidate. Candidate 1 in NGC 6946 had an initial apparent magnitude of $R_c \simeq 21.89$ mag ($\nu L_\nu = 2.7 \times 10^4 L_\odot$). It was observed to have a relatively stable luminosity for two epochs before it experienced an outburst and then faded. Archival *SST* data show a long, slow mid-IR transient is associated with the source but the resolution makes it impossible to securely identify our source. Follow up observations with *HST/SST* and continued monitoring should help better determine the nature of this candidate. Fitting the available data with stellar models and mapping those results onto isochrones imply a red star with a mass of $18M_\odot \lesssim M_* \lesssim 25M_\odot$, placing this candidate in the mass range of the red supergiant problem.

We use the known ccSNe in these galaxies as tests of our approach. Of the 3 massive stars known to have died during our survey period, SN 2009dh, SN 2011dh and SN 2013fh, we select SN 2011dh as a star which has died. The other 2 SNe have not faded sufficiently to be found as vanishing stars. In the future, we will experiment with adding fake candidates. We have not done so as yet, instead focusing on whether we find the deaths of stars in successful SNe, because it is not entirely clear what fake signal to inject. There is a need for additional studies on the observational signatures of failed SNe such as that by Lovegrove & Woosley (2013) and Piro (2013) to allow such calibration studies.

Because we have a remaining candidate failed SN, we consider the constraints on the fraction of core-collapses that lead to a failed SNe if our sample contains 0 or 1 failed SN.

Using a log prior for our fiducial case for the SN survey ($N_{SN} = 4$ discovered over $t_{SN} = 5.0$ years), we find an upper limit on the fraction of massive stars that experience a failed SN of $f \simeq 0.40$ at 90% confidence if we ultimately reject our remaining candidate. If we have discovered a failed SN, the median fraction is $f \simeq 0.30$ with symmetric 90% confidence limits of $0.07 \leq f \leq 0.62$.

The survey is continuing, and we are planning on a minimum survey duration of 10 years. If we conservatively constrain the ccSN rate using the observed numbers from 2000 to 2014 ($t_{SN} = 14$, $N_{SN} = 12$), then if we find no failed ccSNe, the 90% (95%) confidence upper bounds on f is $f < 0.18$ ($f < 0.31$). Similarly, the probabilities of finding a failed SN are 63%, 88% and 97% for $f = 0.1, 0.2$ and 0.3 , respectively. These estimates are somewhat conservative because we did not take into account the improvements in the estimate of the ccSNe rate given the extended temporal baseline. This is a challenging experiment, but it will set interesting limits and the prospects of a revolutionary discovery are good. Of course, if Candidate 1 survives, the revolutionary discovery has already occurred.

ACKNOWLEDGMENTS

We thank T.A. Thompson and J.F. Beacom for comments and discussions. We thank S. Adams for helpful discussions and providing the “Galactic” curve in Figure 16. We thank the OSURC queue observers and the support staff at LBT for helping us obtain these observations. We also thank Stephen Smartt, the referee, for many helpful suggestions which strengthened the paper. Observations have been carried out using the Large Binocular Telescope at Mt. Graham, AZ. The LBT is an international collaboration among institutions in the United States, Italy, and Germany. LBT Corporation partners are the University of Arizona on behalf of the Arizona university system; Istituto Nazionale di Astrofisica, Italy; LBT Beteiligungsgesellschaft, Germany, representing the Max-Planck Society, the Astrophysical Institute Potsdam, and Heidelberg University; the Ohio State University; and The Research Corporation, on behalf of the University of Notre Dame, University of Minnesota, and University of Virginia. Based on observations made with the NASA/ESA Hubble Space Telescope, obtained from the data archive at the Space Telescope Science Institute. STScI is operated by the Association of Universities for Research in Astronomy, Inc. under NASA contract NAS 5-26555. This work is based in part on observations made with the Spitzer Space Telescope, which is operated by the Jet Propulsion Laboratory, California Institute of Technology under a contract with NASA.

REFERENCES

- Adams, S. M., Kochanek, C. S., Beacom, J. F., Vagins, M. R., & Stanek, K. Z. 2013, *ApJ*, 778, 164
- Alard, C. 2000, *A&AS*, 144, 363
- Alard, C., & Lupton, R. H. 1998, *ApJ*, 503, 325
- Alexeyev, E. N., & Alexeyeva, L. N. 2002, *Soviet Journal of Experimental and Theoretical Physics*, 95, 5
- Annibali, F., Aloisi, A., Mack, J., et al. 2008, *AJ*, 135, 1900
- Blanton, M. R., & Roweis, S. 2007, *AJ*, 133, 734
- Botticella, M. T., Pastorello, A., Smartt, S. J., et al. 2009, *MNRAS*, 398, 1041
- Botticella, M. T., Smartt, S. J., Kennicutt, R. C., et al. 2012, *AAP*, 537, A132
- Bressan, A., Marigo, P., Girardi, L., et al. 2012, *MNRAS*, 427, 127
- Brown, J. M., & Woosley, S. E. 2013, *ApJ*, 769, 99
- Castelli, F., & Kurucz, R. L. 2004, *arXiv:astro-ph/0405087*
- Ceillier, T., Eggenberger, P., García, R. A., & Mathis, S. 2012, *Astronomische Nachrichten*, 333, 971
- Clausen, D., Piro, A. L., & Ott, C. D. 2014, *arXiv:1406.4869*
- Dolphin, A. E. 2002, *MNRAS*, 332, 91
- Dopita, M. A., Calzetti, D., Maíz Apellániz, J., et al. 2010, *Ap&SS*, 330, 123
- Drozdovsky, I. O., & Karachentsev, I. D. 2000, *A&AS*, 142, 425
- Elias-Rosa, N., Van Dyk, S. D., Li, W., et al. 2011, *ApJ*, 742, 6
- Elitzur, M., & Ivezić, Ž. 2001, *MNRAS*, 327, 403
- Fausnaugh, M. M., Kochanek, C. S., Gerke, J. R., et al. 2014, *arXiv:1412.2138*
- Gerke, J. R., Kochanek, C. S., Prieto, J. L., Stanek, K. Z., & Macri, L. M. 2011, *ApJ*, 743, 176
- Giallongo, E., Ragazzoni, R., Grazian, A., et al. 2008, *AAP*, 482, 349
- Gammer, S. H., Humphreys, R. M., & Gerke, J. 2015, *arXiv:1502.00308*
- Griga, T., Marulla, A., Grenier, A., et al. 2011, *Central Bureau Electronic Telegrams*, 2736, 1
- Groh, J. H., Meynet, G., Georgy, C., & Ekström, S. 2013, *AAP*, 558, A131
- Heger, A., Fryer, C. L., Woosley, S. E., Langer, N., & Hartmann, D. H. 2003, *ApJ*, 591, 288
- Herrmann, K. A., Ciardullo, R., Feldmeier, J. J., & Vinciguerra, M. 2008, *ApJ*, 683, 630
- Herrnstein, J. R., Moran, J. M., Greenhill, L. J., et al. 1999, *Nature*, 400, 539
- Hill, J. M., Green, R. F., & Slagle, J. H. 2006, *Proc. SPIE*, 6267, 62670Y (2006)
- Hopkins, A. M., & Beacom, J. F. 2006, *ApJ*, 651, 142
- Horiuchi, S., Beacom, J. F., Kochanek, C. S., et al. 2011, *ApJ*, 738, 154
- Horiuchi, S., Nakamura, K., Takiwaki, T., Kotake, K., & Tanaka, M. 2014, *arXiv:1409.0006*
- Ikeda, M., Takeda, A., Fukuda, Y., et al. 2007, *ApJ*, 669, 519
- Ivezic, Z., Nenkova, M., & Elitzur, M. 1999, *arXiv:astro-ph/9910475*
- Ivezić, Ž., et al. 2007, *AJ*, 134, 973
- Jacobs, B. A., Rizzi, L., Tully, R. B., et al. 2009, *AJ*, 138, 332
- Janka, H.-T. 2012, *Annual Review of Nuclear and Particle Science*, 62, 407
- Jennings, Z. G., Williams, B. F., Murphy, J. W., et al. 2012, *ApJ*, 761, 26
- Jennings, Z. G., Williams, B. F., Murphy, J. W., et al. 2014, *arXiv:1410.0018*
- Jordi, K., Grebel, E. K., & Ammon, K. 2006, *AAP*, 460, 339
- Kanbur, S. M., Ngeow, C., Nikolaev, S., Tanvir, N. R., &

- Hendry, M. A. 2003, AAP, 411, 361
- Karachentsev, I. D., Sharina, M. E., & Huchtmeier, W. K. 2000, AAP, 362, 544
- Karachentsev, I. D., Makarov, D. I., Sharina, M. E., et al. 2003, AAP, 398, 479
- Karachentsev, I. D., Karachentseva, V. E., Huchtmeier, W. K., & Makarov, D. I. 2004, AJ, 127, 2031
- Karachentsev, I. D., Dolphin, A., Tully, R. B., et al. 2006, AJ, 131, 1361
- Kennicutt, R. C., Jr., Armus, L., Bendo, G., et al. 2003, PASP, 115, 928
- Khan, R., Kochanek, C. S., Stanek, K. Z., & Gerke, J. 2014, arXiv:1407.7530
- Kochanek, C. S., Beacom, J. F., Kistler, M. D., et al. 2008, ApJ, 684, 1336
- Kochanek, C. S., Szczygiel, D. M., & Stanek, K. Z. 2012a, ApJ, 758, 142
- Kochanek, C. S., Khan, R., & Dai, X. 2012b, ApJ, 759, 20
- Kochanek, C. S. 2014, ApJ, 785, 28
- Kochanek, C. S., Adams, S. M., & Belczynski, K. 2014, arXiv:1405.1042
- Kochanek, C. S. 2014, arXiv:1407.5622
- Kochanek, C. S. 2014, MNRAS, 444, 2043
- Kotake, K. 2011, Journal of Physics Conference Series, 314, 012080
- Lasker, B. M., Lattanzi, M. G., McLean, B. J., et al. 2008, AJ, 136, 735
- Li, W., Bloom, J. S., Podsiadlowski, P., et al. 2011, Nature, 480, 348
- Lien, A., Fields, B. D., & Beacom, J. F. 2010, PRD, 81, 083001
- Lovegrove, E., & Woosley, S. E. 2013, ApJ, 769, 109
- Maeder, A. 1992, AAP, 264, 105
- Marigo, P., Girardi, L., Bressan, A., et al. 2008, AAP, 482, 883
- Maund, J. R., Reilly, E., & Mattila, S. 2014, MNRAS, 438, 938
- Monard, L. A. G. 2009, Central Bureau Electronic Telegrams, 1867, 1 USNO-A2.0 catalog
- Monet, D., Bird, A., Canzian, B., Dahn, C., Guetter, H., Harris, H., Henden, A., Levine, S., Luginbuhl, C., Monet, A. K. B., Rhodes, A., Rieke, B., Sell, S., Stone, R., Vrba, F., & Walker, R. 1998, The USNO-A2.0 Catalogue, (U.S. Naval Observatory, Washington DC).
- Monet, D. G., Levine, S. E., Canzian, B., et al. 2003, AJ, 125, 984
- Mühlbeier, T., Nunokawa, H., & Funchal, R. Z. 2013, PRD, 88, 085010
- Nadezhin, D. K. 1980, Ap&SS, 69, 115
- Nakano, S., Yusa, T., Yoshimoto, K., et al. 2012, Central Bureau Electronic Telegrams, 3263, 1
- Nugent, P. E., Sullivan, M., Cenko, S. B., et al. 2011, Nature, 480, 344
- O'Connor, E., & Ott, C. D. 2011, ApJ, 730, 70
- Ott, C. D. 2009, Classical and Quantum Gravity, 26, 204015
- Pejcha, O., & Thompson, T. A. 2014, arXiv:1409.0540
- Piro, A. L. 2013, ApJL, 768, L14
- Poznanski, D., Butler, N., Filippenko, A. V., et al. 2009, ApJ, 694, 1067
- Prantzos, N. 1994, AAP, 284, 477
- Prieto, J. L., Stanek, K. Z., Kochanek, C. S., et al. 2008, ApJL, 673, L59
- Prieto, J. L., Kistler, M. D., Thompson, T. A., et al. 2008, ApJL, 681, L9
- Sahu, D. K., Anupama, G. C., Srividya, S., & Muneer, S. 2006, MNRAS, 372, 1315
- Schlafly, E. F., & Finkbeiner, D. P. 2011, ApJ, 737, 103
- Shappee, B. J., & Stanek, K. Z. 2011, ApJ, 733, 124
- Smartt, S. J., Eldridge, J. J., Crockett, R. M., & Maund, J. R. 2009, MNRAS, 395, 1409
- Smartt, S. J. 2009, ARA&A, 47, 63
- Smartt, S. J., Smith, K. W., Wright, D., et al. 2014, Central Bureau Electronic Telegrams, 3876, 1
- Szczygiel, D. M., Gerke, J. R., Kochanek, C. S., & Stanek, K. Z. 2012, ApJ, 747, 23
- Theureau, G., Hanski, M. O., Coudreau, N., Hallet, N., & Martin, J.-M. 2007, AAP, 465, 71
- Thim, F., Hoessel, J. G., Saha, A., et al. 2004, AJ, 127, 2322
- Tonry, J. L., Dressler, A., Blakeslee, J. P., et al. 2001, ApJ, 546, 681
- Tsvetkov, D. Y., Pavlyuk, N. N., & Bartunov, O. S. 2004, Astronomy Letters, 30, 729
- Ugliko, M., Janka, H.-T., Marek, A., & Arcones, A. 2012, ApJ, 757, 69
- Valenti, S., Sand, D., Howell, D. A., et al. 2013, The Astronomer's Telegram, 5228, 1
- Verdes-Montenegro, L., Bosma, A., & Athanassoula, E. 2000, AAP, 356, 827
- Walmswell, J. J., & Eldridge, J. J. 2012, MNRAS, 419, 2054
- Welch, D. L., Clayton, G. C., Campbell, A., et al. 2007, ApJ, 669, 525
- Williams, B. F., Peterson, S., Murphy, J., et al. 2014, arXiv:1405.6626
- Willick, J. A., Courteau, S., Faber, S. M., et al. 1997, ApJS, 109, 333
- Woosley, S. E. 1993, ApJ, 405, 273
- Woosley, S. E., & Heger, A. 2012, ApJ, 752, 32